Review

Nanoparticles Processed from Agricultural Waste Biomass—A Review

Shadrack Mubanga Chisenga * , Francis Collins Muga , Olabisi Mariam Okesola , Jones Yengwe , Haibao Liu , Peter Kaluba , Alice Mutiti Mweetwa , Zizikazi Sodzidzi

Posted Date: 10 February 2026

doi: 10.20944/preprints202602.0729.v1

Keywords: waste biomass; lignocellulose; cellulose; carbonized particles; nanocellulose; rheology, thermal decomposition; crystallinity; Zeta potential

 doi:10.20944/preprints202602.0729.v1

Review

Nanoparticles Processed from Agricultural Waste Biomass—A Review

Shadrack Mubanga Chisenga [1,2,*], Francis Collins Muga [3], Olabisi Mariam Okesola [3], Jones Yengwe [1], Haibao Liu [2], Peter Kaluba [1], Alice Mutiti Mweetwa [1] and Zizikazi Sodzidzi [3]

[1] Department of Land Management, School of Agricultural Sciences, University of Zambia, P O Box 32379, Lusaka, Zambia

[2] School of Engineering and Materials Science, Queen Mary University of London, London, United Kingdom

[3] Department of Agricultural and Rural Engineering, Faculty of Science Engineering and Agriculture, University of Venda, Private Bag X5050, Thohoyandou, South

* Correspondence: mubanga.chisenga@univen.ac.za

Abstract

The nanoparticles processed from non-edible crop materials and residues have evoked great use in the food and non-food industry. The diversity in agricultural waste biomass and differences in extraction techniques account for variations in end-product properties, and would require examination of waste crop types (source) for suitability of production of cellulose, and nanocellulose including graphene particles. This review showed that screening criteria of end-user properties include chemical composition, cellulose contents, morphology, crystallinity, thermal stability, rheology, surface charge and zeta potential. Literature shows that the end-user properties vary with plant source (that is crop type) and extraction techniques. In this review, the cellulose content and percentage crystallinity are primary parameters for selecting agricultural waste biomass for production of nanocellulose and nanofibrils. Additionally, zeta potential and surface charge can determine polymer interaction for suitability of industrial applications. Moreover, nanocellulose including biochar were found to have various industrial application as ingredients in production of food packaging including active packaging, rheological modifiers and thickeners. Pyrosis is eminently the strategy for transformation of agricultural waste into biochar-derived nanoparticles and carbon-rich materials.

Keywords: waste biomass; lignocellulose; cellulose; carbonized particles; nanocellulose; rheology, thermal decomposition; crystallinity; Zeta potential

1. Introduction

Agricultural waste comprised of non-edible and non-usable parts of food and non-food crops, including crop residues (straw, stalks, husks, leaves) and animal manure. The global production of major crops was estimated to produce over 16 billion tonnes of total biomass annually, of which ~80-85% as non-edible residues [1]. The objectives for higher yielding crop varieties, would suggest increasing amount of amount of agricultural waste biomass. The increasing waste biomass has emerged as a concerning issue in many countries including South Africa and the broader Southern African region, where approximately 90% of general waste consists of biodegradable materials from food and non-food plant sources. The agricultural waste accounts for a large proportional of landfill materials and prominently becoming a major environmental and economic concern. The concerns on rising greenhouse gases were ascribed to the increasing agricultural waste [2]. Nonetheless, there has been a growing trend towards utilizing agricultural waste to develop value added products based on biopolymers [3-5]. The industrial efforts towards valorisation of agricultural waste has been centred on lignocellulosic biomass.

 doi:10.20944/preprints202602.0729.v1

Lignocellulose biomass is a complex molecular of biopolymers, environmentally friendly and the most abundant renewable natural material derived from agricultural waste and forestry residues. Lignocellulose is component of three major biopolymers of cellulose, hemicellulose, and lignin. These three major biopolymers are highly fibrous structures of the plant cell wall [6]. The crude contents by weight of cellulose, hemicellulose, and lignin were reported in the range of ~35-55%, 20-40%, and 10-25%, respectively. The differences in composition and the content of these biopolymers can vary according to species, germplasm types and planting season [7] including methods of treatment and extraction techniques. The recalcitrance of lignin can limit transformation of biomass into valuable products such bioethanol. Lignin has 3D structural network of phenylpropanoid units linked by ether and carbon-carbon bonds exhibiting a high molecular weight and densely of hydrophobic nature. This structure complex was reported to hinder chemical or enzyme access to cellulose and hemicellulose, making difficult to fractionate lignocellulose. In view of this, several extraction methods have been developed with a common goal of removing lignin to produce holocellulose (molecular structure of hemicellulose and cellulose together).

Cellulose is the major component of lignocellulose biomass, and can be extracted using alkaline and acid hydrolysis, and bleaching processes. Cellulose including raw lignocellulose materials can be pyrolyzed onto biochar and carbon graphene particles, and can be activated using various processes such as acid and alkaline treatment including particle size reduction. Increasing demand for nano-scale sustainable materials and ingredients has elicited greater research interest in production of nanomaterials from plant sources. Cellulose can be processed into nanocellulose and cellulose nanofibrils. This paper catalogues chemical composition of raw agricultural waste biomass, processes for extraction of cellulose, and production of nanocellulose and biochar. Also, the paper interprets and explain the variations in nanocellulose properties such as surface charge, crystallinity, thermal stability, and zeta potential.

2. Composition and Extraction of Lignocelluloses

The composition of various agricultural waste materials is shown in Table 1. The agricultural waste biomass is the rich source of lignocellulose, a polysaccharide containing cellulose, hemicellulose and lignin.

2.1. Lignin Content

Highest lignin content (40%) were shown in olive leaf, making it significant source of lignocellulose while olive wood and pruning parts yielded lower amounts of lignin [8]. This is indicative of variation in lignin content across different parts of the same the plant. Lignin is phenolic polymer with amorphous structure of three monomers, guaiacyl propane, syringyl propane, and 4-hydroxyphenylpropane [9], which are chemically cross-linked through alkyl-ether, carbon-carbon and aryl-ether bonds, and play functional role of binding cellulose and hemicellulose into holocellulose. The organic solvent and alkali treatment processes are some of the common extraction methods for valorising lignin into useful products. The reactive sites of the phenol ring interact with formaldehyde producing hydroxymethyl phenols linked through methylene bridges (C-C) and ether bridges (C-O-C) to form cross-linked and rigid structural network. This mechanism signifies the role of pure lignin for industrial applications including synthesis of emulsifiers, additives and phenolic resins [10, 11]. Yet, there is limited scientific investigation on utilization of lignin in production of sustainable ingredients. The higher removal rate of lignin from lignocellulose can result into increased concentration of holocellulose (hemicellulose and cellulose).

Table 1. Cellulose, lignin and hemicellulose contents of agricultural waste biomass.

Fibrous Biomass	Cellulose	Lignin	Hemicellulose	Treatment/Extraction Process	Reference
Rice husk	30-70	3-25	10-20	Alkaline, bleaching agent, acid hydrolysis	Hafid, H.S. et al. [125]

 doi:10.20944/preprints202602.0729.v1

Rice husk	50	27	10	NaOH treatment, water washing	Ponce, J. et al. [126]
Rice husk	22-57	-	-	Acetic acid, bleaching ($NaOH/H_2O_2$)	Vu, A.N. et al. [127]
Rice husk	16	21	36	Removal of dust, without treatments	Lin, L. et al. [128]
Rice straw	18	14	47	Removal of dust, without treatments	Lin, L. et al. [128]
Sugarcane bagasse	58	12	17	NaOH treatment, water washing	Ponce, J. et al. [126]
Sugarcane bagasse	39	26	24	Acid hydrolysis	Rodríguez-Chong, A. et al. [129]
Sugarcane bagasse	26-47	19-23	14-23	Alkaline treatment, hot water wash	Mahmud, M.A. and Anannya, F.R. [130]
Sugarcane bagasse	41	23	21	High temperature alkaline treatment	Song, G. et al. [131]
Peanut shell	36-59	27	7	Deep eutectic solvents	Lu, A. et al. [30]
Peanut shell	32-34	32	18	Standard and extraction methods	Husna, M. and Vasantharuba, S. [132]
Peanut shell	32-37	27-30	7-9	Inoculum of culture incubation process	Anike, F. et al. [133]
Peanut shell	45	36	6	-	Pączkowski, P. et al. [134]
Corn husk	55	9	27	NaOH treatment, water washing	Ponce, J. et al. [126]
Corn stalk	38-44	5-10	17-27	Inoculum of culture incubation process	Anike, F. et al. [133]
Corn bract	36	39	15	Enzymatic hydrolysis without pre-treatment	Anike, F. et al. [133]
Corn bract	52	35	4	Acetic acid, enzymatic hydrolysis	Anike, F. et al. [133]
Corn bract	76	13	2	Ammonium, enzymatic hydrolysis	Anike, F. et al. [133]
Olive leaves	6-9	40	4-9	Acid hydrolysis	Garcia-Maraver, A. et al. [135]
Olive pruning	20	27	10-11	Acid hydrolysis	Garcia-Maraver, A. et al. [135]
Olive wood	31-32	24	11-15	Acid hydrolysis	Garcia-Maraver, A. et al. [135]
Pineapple leaf	30	22	37	NaOH and sodium chlorite treatment	Mansora, A.M. et al. [136]
Pineapple leaf	66	4	20	Bleaching agent	Daud, Z. et al. [137]
Pineapple stem	37	20	34	NaOH and sodium chlorite treatment	Mansora, A.M. et al. [136]
Pineapple root	42	19	32	NaOH and sodium chlorite treatment	Mansora, A.M. et al. [136]
Banana stem	35	12	25	NaOH and sodium chlorite treatment	Mansora, A.M. et al. [136]
Banana stem (outer)	40	13	25	NaOH and sodium chlorite treatment	Mansora, A.M. et al. [136]
Cassava peel	38	8	37	Dust removal, without treatment	Aripin, A.M. et al. [138]
Cassava peel	40	12	21	Dust removal, without treatment	Aripin, A.M. et al. [138]
Cassava peel	38	8	37	Bleaching agent	Daud, Z. et al. [137]

2.2. Hemicellulose Content

Hemicellulose is heterogeneous polymers of various monomers including pentoses and hexoses sugars such as xylose, mannose, and glucose. Hemicellulose varied in the range of about 10–40% across different agricultural biomass. The xylan monomers are abundant in hardwood [12] and this can explain the higher hemicellulose content (40%) in rice straw than rice husk. In the plant cell wall, hemicellulose is bonded with cellulose fibrils through lignin cross-links of hydrogen bonds and Van der Waals forces [13]. Hemicellulose can be extracted or removed from the biomass through various hydrolysis methods using acid and alkaline treatment, and enzymatic processes. The hemicelluloses extracted from different biomass including bamboo using mild alkaline treatment showed diverse monosaccharide composition predominantly containing xylose [14]. Pure hemicellulose can alter its properties for specific applications such as increasing hydrophobicity and thermal stability through etherification, esterification, or cross-linking. These properties give hemicellulose has wide range of industrial applications including biodegradable films and coatings for food packaging [15].

2.3. Cellulose Content

 doi:10.20944/preprints202602.0729.v1

Cellulose [$(C_6H_{10}O_5)n$] is the most abundant and major polysaccharide of glucose in plants, and serving a structural function rather than nutritional role. It is unbranched polymer (linear polysaccharide structure) of glucose residues joined by β(1-4)-glycoside linkages [16]. The structural (residue) of the chain is D-glucopyranosyl units. The β-configuration allows cellulose to form very long, straight chain of repeated units of D-glucopyranosyl units. The contents of cellulose varied in the range of about 20-85% across different agricultural waste biomass. The amount cellulose by weight were greater than those hemicellulose and lignin, making it the major component of lignocellulosic biomass. The differences in crude content of cellulose were ascribed to germplasm of plant species, plant age, geographical origin, and season of planting [17]. The D-glucopyranosyl has hydroxyl functional groups responsible for hydrogen bonding within the same linear structure and with monomers of other different carbon chain. Cellulose fibrils can be formed when parallel chains interact through hydrogen bonding. This creates entangled network of intramolecular and intermolecular hydrogen bonding into a tightly packed crystalline and fibrous structure. The straight chain formed by β linkages combined with structural entanglement can explain the high tensile strength in fibres [16, 18]. The cellulose fibrils were characterized to undergo thermal decomposition at high temperatures in the range of 300-315^{o}C. This thermal stability heightens the use of cellulose in the production of sustainable industrial lightweight products and nanoparticles [19]. The high rate removal of lignin and hemicellulose proportionately increases the yield of cellulose. Cellulose can be extracted using conversional pulping methods including Kraft, sulphite and bleaching processes. Kraft pulping is an alkaline treatment, and in combination with mixture of sodium hydroxide and sodium sulphide, the method yielded 72-85% of cellulose from sugarcane bagasse [20]. Sulphite method is acid hydrolysis, commonly using sulfuric acid and was reported to reduce 88% lignin by volume while retaining 92% of extracted cellulose fibres [21]. Bleaching agents such as chlorine-based chemicals including hydrogen peroxide and sodium chlorite are added to the extracted cellulose for the purposes of increasing the whiteness index of cellulose. Additionally, bleaching agents have additional role of degrading the amorphous region of cellulose [22, 23]. It is worth noting that pure cellulose is extracted cellulose less its ash content. Please see the work of Zhang, M. et al. [24] on calculating percentage cellulose adjusted against the content of its ash.

Cellulose can be classified into four allomorphs cellulose types I, II, III, and IV. The differences lie in crystalline forms based on the arrangements of cellobiose units (D-glucopyranosyl) in the chain and hydrogen bonding patterns [25]. Cellulose type I is the native cellulose mainly a combination of two co-existing crystal structures named I_α and I_β, of which I_β is the major component in higher plants, and have parallel packaging structure of hydrogen-bonds [26]. Cellulose type II exhibited antiparallel packing of hydrogen-bonding due to chemical modification of native cellulose when treated in alkaline or acid hydrolysis. Cellulose type III is generated by treating native cellulose or cellulose II in liquid ammonia or other amines [27]. Cellulose type IV is generated using physical modification in which Cellulose III or Cellulose II is heated at temperatures of about 300^{o}C in plasticizing liquid medium such as glycerol. Cellulose IV showed high thermal stability at higher temperatures and this can explain its desired application in the production of high-grade cellulose fibres used in rayon manufacturing [28]. This showed that raw native cellulose can have limited applications, and would require that cellulose is functionalized using physical and chemical modifications. However, sustainable methods are desired in response to climate change objectives.

3. Green Methods for Extraction of Cellulose

Green methods for cellulose extraction are aimed at environmentally friendly compounds and energy-efficient techniques. Although green methods are cost prohibitive and time consuming, are reported to offer sustainable approaches for extraction of cellulose from agricultural waste biomass. Some of the common sustainable methods included ionic liquid solvents and enzymes.

3.1. Ionic Liquid Solvents

 doi:10.20944/preprints202602.0729.v1

Increasing environment safety concerns due to the use of hazardous chemicals led to development of green methods, some of which included ionic liquid solvents made of organic salts that are liquid at or near room temperature [29]. Imidazolium based ionic liquids including 1-Dodecyl-3-methyl-imidazolium, 1-Decyl-3-methyl-imidazolium, tetra-butyl-phosphonium acetate and tri-butyl-methyl-phosphonium acetate were reported to dissolve corn stover yielding huge amount of cellulose in range of 44-84% of [19] under mild conditions of 80°C, 3h [19]. The deep eutectic solvent composed of choline chloride and guaiacol in the 1:1 molar ratio was used to dissolve peanut shell resulting in high yields of 60% cellulose with reduction of lignin and hemicellulose at removal rates 70% and 90%, respectively [30]. Nevertheless, high viscosity of ionic liquids can limit mass transfer rate resulting in decreased reaction and absorption rates [31], and attempts to increase pump force to aid mass transfer can be cost probative. Other associated challenges included high cost of production. The lack of standardized regulations can limit application of ionic liquids at scale.

3.2. Enzymatic Process

The extraction of cellulose using enzymatic hydrolysis is commonly a multi-step process using ligninase enzymes such as laccase and lignin peroxidase to degrade lignin; and hemicellulose enzymes such as xylanase to breakdown hemicellulose [32, 33]. The digested lignin and hemicellulose can be separated from cellulose through filtration and washing [34]. The enzymatic system for cellulose extraction can be a blend of enzymes having different mechanisms of action that result into degradation of lignin and hemicellulose, and retention of cellulose [35]. The enzymes for cellulose extraction processes are microbial nature, and commercially available. The ligninase (CAS: 80498-15-3) is the lactase responsible for catalysing the oxidation of phenol containing compounds through the reduction of oxygen to water [36]. The pectinase (CAS: 9032-75-1) has functional role of breaking down the polysaccharide pectin [36], and aiding liquefaction processes by reducing viscosity for improved filtration and product clarity, and preventing particle sedimentation [37]. The hemicellulase (CAS: 9025-56-3) is a glycoside hydrolase [36] with a functional role of hydrolyzing the bonds in heteropolysaccharides like xylan and mannan, and converting complex plant fibers into simpler sugars [38, 39]. The enzymes of fungal species for aiding production of cellulose included *Penicillium verruculosum, Trichoderma reesei, Aspergillus niger, Sporotrichum Thermophile* [40]. However, the fibrous structural properties of various biomass feedstock are resistant to enzymatic hydrolysis. The interaction of lignin and hemicellulose through covalent/non-covalent bonds can form rigid structure that limits enzymatic access to the lignin [41]. To overcome these drawbacks, prior addition of enzymes, the primary step is pre-treatment process such as milling, boiling or heating aimed at degrading hemicellulose. Also, soaking in water can allow material sample to imbibe water molecules, resulting in expanded structure and thus, increasing enzymatic accessibility. Additionally, soaking releases impurities which would otherwise hinder enzymatic performance. The most of pre-treatment methods were selectively targeted at hemicellulose because of its lower degree of polymerization, make it an ease component to degrade. Yuan, X. et al. [42], demonstrated that enzymatic hydrolysis of corn bract pre-treated in ammonia peroxide mixture (NH_3/H_2O_2) yielded higher cellulose content (76%) compared to cellulose content (52%) from glacial acetic acid (CH_3COOH/H_2O_2) pre-treated corn bract (Table 1). Additionally, NH_3-enzymatic hydrolysis showed higher removal rate of 86% and 70% of lignin and hemicellulose, respectively [42]. Ammonia carries amine functional group that can disrupt the hydrogen bonds linking hemicellulose with other biomass components, resulting in increased accessibility for enzymatic action leading to improved extraction of cellulose [42, 43].

4. Production of Nanoparticles

Producing nanoparticles from agricultural waste biomass through carbonization processes represents a sustainable approach to valorise abundant, low-cost residues like crop husks and peels into high-value nanomaterials. The nanocellulose is extracted from cellulose fibrils using various

 doi:10.20944/preprints202602.0729.v1

extraction methods. The major production methods of nanoparticles included carbonization, acid hydrolysis, enzymatic hydrolysis and mechanical process.

4.1. Carbonization

Carbonization is the thermal decomposition of biomass in oxygen-limited conditions to yield carbon-rich structures at the nanoscale with reactive properties such as high surface area and porosity. The techniques include pyrolysis, hydrothermal carbonization, and microwave-assisted carbonization. These processes are combined with activation steps for improved particle functionality. The raw waste biomass is prepared by screening and sorting to remove the foreign matter. The sorted biomass is washed using industrial water, with subsequent washing using deionized water, and drying at temperature of 65–110°C. Drying at low temperatures (45-65^{o}C) is aimed at maintaining the native biomatrix structure of lignocellulose. The dried biomass is ground into powder to reduce the particle size.

Pyrolysis is the common thermochemical technique of carbonization in which biomass is thermally decomposed into biochar when heated at temperature range 300–1300°C under inert gas conditions in the furnace [44]. The resulting product is biochar, a carbon-rich, but mostly amorphous [45]. The typical process utilizes carbon dioxide and a mixture of other inert gases including nitrogen, methane, hydrogen. The choice of heating temperature is prescribed by thermal properties of biomass. The common methods of pyrolysis are classified into slow, fast and gasification. The slow pyrolysis is characteristic of low heating rates (5–7°C min^{-1}) at temperature range of 400–650°C with higher residence times from hours to days [46]. This process can yield biochar 35-50% of biomass weight with higher carbon content (70–80%). The fast pyrolysis operates in the temperature range of 800–1250°C with heating rates (10–200°C sec^{-1}), and short residence times (1–5 sec), and can yield higher bio-oil (60–75%) than biochar (10-25%), and have higher surface area [47]. However, fast pyrolysis was associated with biochar of lower carbon stability due to rapid volatilization.

Steam pyrolysis is conducted using biomass reactor for production of various products including hydrogen, bio-oil and char [48]. The biomass reactor is heated to 100^{o}C followed by injection of steam and nitrogen gas at rate of 2 mL $H_2O_{(g)}$ min^{-1} and 30 mL min^{-1}, respectively. The generated liquid products are collected in a glass liner located in a cold trap maintained at 0^{o}C. The liquid phase consisting of an aqueous and an oil phase can be fractionated to yield bio-oil. The steam pyrolysis of cotton seedcake using Heinze reactor with steam velocity 2.7 cm sec^{-1} at various temperatures 400-700^{o}C yielded maximum char (27%) and oil (39%) at 400^{o}C and 550^{o}C, respectively [49]. The low yields of biochar (17-22%) at higher temperatures (>400^{o}C) is indicative of increased secondary reactions as pyrosis temperature increased. Nonetheless, the steam process can yield natural porous structure of the biochar with surface area as high as 1000 m^{2}g^{-1} (Table 2).

4.2. Biochar Activation

The activation of biochar involves chemical treatments, and physical methods primarily drying and milling processes to form various allotropes of carbon including fullerene, graphene, carbon nanotubes, and carbon nanofibers, graphene-like nanosheets (Table 2). The activation is aimed at removing non-carbon components like O and H to yield a structure with improved porosity and surface area with increased carbon purity.

Table 2. Production of nanoparticles from lignocellulose and cellulose .

Nanomaterial	Material	Method	Activation Process	Surface Effect	Reference
Graphene	Rice husk	Carbonization Pyrosis 400 ^{o}C	Mixture of biochar with KOH in 1:2 ratio. annealing at 800^{o}C, washing and drying	few-layered graphene with agglomeration of silica particles (porous)	Mubarik, S. et al. [139]
Graphene	Peanut shells	Carbonization Pyrosis 200 ^{o}C	Mixture of biochar and $FeCl_3.6H_2O$ in water. Adjust pH HCl (98% Betaine Hydrochloride). Washing and drying at 100^{o}C, milling	Two-dimensional (2D) material, network of SP^2-bonded carbon atoms	Aro-Modiu, O. et al. [50]

 doi:10.20944/preprints202602.0729.v1

Graphene oxide	Graphene	-	Mixture of graphene powder, sodium nitrate and H_2SO_4 in ice bath. Adding $KMnO_4$. Reaction termination with H_2O_2. washing, filtration. Drying 30°C.	Polar groups (surface HO^- groups), surface area≈2630 $m^2 g^{-1}$.	Aro-Modiu, O. et al. [50] [140]
Graphene	Rubber seed shell	Pyrolysis 700 °C 90 min	Mixture of biochar to KOH in 1:3 ratio forunder N_2 at different temperatures (600, 700, 800 and 900°C), 3h	Surface area 712 m^2g^{-1}	Anthonysamy, S. et al. [52]
cellulose nanocrystals	Peanut shells	lignocellulose	Peanut shell powder (500-µm sieve), hot rinse and dry. Treatment: HCl, NaOH. precipitate washed, centrifuged. Residual fibres sonicated and dried. Fibres hydrolysed with H_2SO_4, cold water wash, centrifuge, ultrasonication, drying	High antifungal and antibacterial activity. positive reaction and sensitivity against Gram (−) and Gram (+) strains of pathogens	Terea, H. et al. [141]
Cellulose nanocrystal	Tea leaf waste fiber	Cellulose extraction	Acid hydrolysis: cellulose treated with H_2SO_4 (pre-heated). Processes of- dialysis of suspension and ultrasonic.		Abdul Rahman, N.H. et al. [142]
Nanocellulose crystals	Tea stalk	Cellulose isolation	Acid hydrolysis	Lower zeta (ζ) potential -33 mV	Guo, Y. et al. [143]
Nanoparticles	Cassava peel	Starch extraction,	Sulphuric acid hydrolysis, washing and drying		Abdul Rahman, N.H. et al. [144]
Silica Nanoparticles	Sugarcane bagasse	Extraction, precipitation	Acid hydrolysis, alkali hydrolysis	surface area 111 m^2g^{-1}	Mohd, N.K. et al. [145]
Cellulose nanofibers	Banana peel		Alkaline hydrolysis (KOH), bleaching ($NaClO_2$), acid hydrolysis (H_2SO_4) Mechanical process: two-stage high-pressure homogenizer	Between -16 mV and -44 mV	Pelissari, F.M. et al. [146]

The common chemical agents are potassium hydroxide, potassium ferrate, metal catalysts such iron, cobalt and nickel, and acids like sulfuric acid and phosphoric acid. The mixture of biochar and chemical agent can heated at various temperatures. Aro-Modiu, O. et al. [50], demonstrated conversion of peanut shell carbonized powder to graphite by impregnating Iron (III) Chloride Hexahydrate ($FeCl_3 \cdot 6H_2O$) on carbonized powder, and pH adjusted using hydrochloric acid. The mixture of which stirred and heated at 60°C for 5 h, and was left to undergo gradual evaporation for 7 days and final drying at 100°C, 1 h using air circulation oven. This process yielded 95% of graphene based on 2g biochar [50]. Iron (Fe) acted as a catalyst by dissolving carbon and precipitating graphene structures. The chloride (Cl^-) interacts with carbon and non-carbon components which increases surface area and porosity for enhanced adsorption capabilities [51]. The alkali (KOH)-activated biochar showed higher adsorption capacity by capturing environmental pollutants at rate of 63-87 mg g^{-1} of nitric oxide than native form of biochar at 18 mg g^{-1} [52]. Potassium interacts with biochar structure between the carbon layers, creating forces that disperse the layers apart leading to formation of tiny space (pores) and thus increasing porosity; and OH^- group introduced more oxygen-containing functional groups and thus improved surface chemistry. Anthonysamy, S. et al. [52], demonstrated that increasing amount of alkali impregnation on a unit biochar weight basis from 1:1 to 3:1 yielded increased surface area of graphene from 390 to 712 $m^2 g^{-1}$, the positive change in surface chemistry of which, can be ascribed to enhanced interactions of oxygen with carbon, and this can increase formation of carboxyl group, hydroxyl group and epoxy groups.

Acid activation can impact on the physicochemical properties of biochar by creating acid functional groups on the biochar. The acid hydrolysis is aimed at removing the metallic impurities, and introduces new functional groups in the inner pores and on the surface and building negatively charged surface areas, and thus modifying the physicochemical properties of biochar [53]. Some of the commonly utilized acidic agents included sulphuric acid, hydrochloric acid, nitric acid, oxalic acid, phosphorous acid and citric acid [54]. However, the environment safety concerns led to growing interest in green chemistry principles in reference to principle 3-less hazardous synthesis [55]. In view of this, organic acids such as carboxylic acid (-COOH) can be used to functionalize biochar. Some of the common organic acids containing -COOH functional groups are acetic acid, citric acid, tartaric

 doi:10.20944/preprints202602.0729.v1

acid, oxalic acid and malic acid [56]. Carboxylic functionalized biochar can find various applications including catalysis and biochar supported nanostructures.

4.3. Production of Nanocellulose

The extracted cellulose finds application as feedstock in the production of nanoparticles of biological nature derived from natural fibres. The nanocellulose materials are classified as nanofibers, nanocrystal, nanofibrillated, and nanocrystalline (Table 2). The other category is bacterial cellulose nanocrystal, however, the present work focussed on nanomaterials of plant origin. The nanomaterials can be differentiated based on source and morphology (size, shape, form) including aspect ratio. Both nanofibers and nanocrystals processed are from cellulose and exhibited at least one dimension in the range 1–100 nm, however, nanofibers showed higher aspect ratio than nanocrystals. The nanofibrillated materials composed of cellulose nanofibers in the form of a gel or film. Similarly, nanocrystalline materials composed of cellulose nanocrystals in the form of a gel, film, or membrane. Milling is the size reduction process and the key activity in the production of nanoparticle and activation process. The milling process-assisted technologies included ultrasound of ultrasonication, high-pressure homogenization, and microwave [57]. Other mill process-assisted techniques included hydrolysis of acidic, alkaline, water or alcohol nature. Organic solvents-assisted ball milling can be used in production of nanocellulose.

4.4. Mechanical Milling

Ball milling is the mechanical process of grinding materials into finest powders at the nanoscale. The mechanical method uses high shear forces in the range 20–30 kWh kg^{-1} to break down fibres into fibrils (Table 3). The equipment is primarily made of cylindrical jar packed with balls. The balls are made of durable materials such steel or ceramic. The cylindrical jars are designed to rotate. The milling machine with stationary housing (cylindrical jars) with an impeller attachment of rotating arm inside the cylindrical jar, are commercially known as attritor mill or stirred ball mill. The rotating arm or jar causes motion among the balls resulting in shearing or colliding of ball against each other and the housing walls, and this action releases energy required to transform the particles from micro size to nanoscale. This mechanism in presence of the sample material causes impact, compression and shear forces for not only particle size reduction, but also for mixing and blending the materials. This mechanical milling as a material processing technology for nanomaterials has wider applications in various industrial areas including pharmaceutical, bioengineering, and packaging. The technology does not require use of strong chemical agents, and has been described as environmentally safe method. Nonetheless, there is a serious challenge relating to reproducible of nanomaterials at scale, specifically, difficulties in predicting milling conditions and suitability for material refinement. Additionally, high times, high energy requirements or low sample quantity per process including contamination, amorphization and stability of nanoparticles are significant challenges limiting commercialization of laboratory experiments for large-scale production of nanopowders. The decrease of crystallinity and undesirable change in crystalline lattice were common challenges associated with ball-milled cellulose. In view of this, much of the recent authored works focused on process optimization in function of independent variables (number and size of balls, time, rotational speed and weight of material). Other variables included status of milling (dry or wet), the weight ratio between balls and material sample.

The types of ball millers commonly used in the industry and laboratory included planetary ball mill, mixer ball mill, and vibration ball mill [58]. The planetary ball mill has been extensively reported for processes of defibrillation of cellulose and lignocellulose biomass. The common speed of ball milling was reported in the range 200 – 700 rpm and time range of 0.5 – 20 h as tabulated in (Table 3). The higher speed can accelerate size reduction and fibrillation compared to lower speeds. Naghdi, M. et al. [59], studied the characteristics of biochar-derived nanoparticles after ball milling using designed experiment based on variation in the key factors of time, rotational speed and ball to powder mass ratio. The result showed that combination of higher rotational speed and short time

 doi:10.20944/preprints202602.0729.v1

(575 rpm, 1.6 h) generated finest particles of 212 nm compared to powder with 453 nm obtained from an experiment of lower rotor speed and high time (540 rpm, 7 h). The high rotation speed can generate high collision energy resulting in reduced milling time. However, dry milling combined with high friction energy can cause overheating which can damage microfibrils. To prevent overheating, the rationing of machine power over milling times was demonstrated [59] by setting the machine on and off at time intervals of 5 min to facilitate heat dissipation. Other works reported the resting phase of 10 min in the cycles of 20 min of milling for the rotor speed of 400 rpm for 3 h, and this implied minimum of five times resting phases in 3 h [60]. The resting period minimizes degradation of crystalline region of cellulose that could possibly occur with continuous milling. The alkali and bleaching pre-treatments of cellulose combined with alkaline-assisted milling, yielded cellulose nanofibrils with higher crystallinity and lower crystal size D-values of 3 nm than those processed from water pre-treatment dry ball milling [60]. Phanthong, P. et al. [61], investigated the properties of cellulose after ball milling with different time treatment (0.5, 1, 2, and 3 h) at 300 rpm. The result showed that increase of ball milling time decreased crystallinity and reduced crystal size of ball-milled cellulose. Crystallinity index decreases exponentially with time due to disrupted hydrogen bonds and polymorph transformation from native cellulose allomorph type I to cellulose type II. The decreased crystallinity can be associated with the increased in amorphous region, and yield of nanocellulose increased with milling time. The milling time is the driving factor for structural disruption and size reduction, and can lead to agglomeration. The decreased crystallinity, increased amorphous region, and consequent agglomeration were commonly associated with dry milling. It is worth noting that the mechanical milling process is not selective because it impacts on both crystalline and amorphous structures, causing some damage to the crystalline domain. The effect wet milling using solvents in ball miller aimed at minimizing loss of crystalline region was investigated. dos Santos, D.F. et al. [62] ascribed the increase in crystallinity to the combination of ethanol-assisted wet milling, longer hours, and low speed. This optimal condition resulted in better fibrillation. Ethanol can cause swelling of the ground matrix, making the structure accessible and accelerate removal of amorphous region and water, including non-cellulose components such as lipids. The ethanol-cellulose interaction is based on hydroxyl groups (OH^-) forming hydrogen bond between molecules, and this action can cause precipitation of nanocellulose.

Table 3. Different techniques and types of ball milling.

Type of Ball Mills	Source & Specification	Process-input	Sample	Primary Properties	Reference
Planetary Mill	PM100; Retsch Corporation, stainless Ballsteel jar (500 mL), stainless steel balls 2.4 mm in diameter x 800 balls	settings at 5 min ON and 5 min OFF Milling speed of 510-630 rpm	Pinewood Biochar, initial size of around 3 mm.	Fine powder 212 - 453 nm Zeta potential (mV) −31.3 ± 2.6	Naghdi, M. et al. [59]
Planetary ball mill	ITO LP-1. 80 mL of jar with different diameters of 10, 5, and 2 mm x 5, 4, and 3 balls, respectively	Speed of 300 rpm, balltime treatment 0.5, 1, 2, and 3 h, acid hydrolysis-assisted	Grade 3 mm Chr cellulose 38 µmI, size (400 mesh) size of cellulose powder	Yield 77-90%, native cellulose type decomposition temperature 300–330 °C with mass loss 75 wt%	Phanthong, P. et al. [61]
Tumbler Mill Ballalumina balls. Jar 1 L	MA500, Marconi, with 70 % of balls and 30 % samples	speed 200 rpm, Treatment times: 1 h, 2 h, 3 h, and 4 h. ethanol-ultrasonic-assisted	Cellulose extracted from eucalyptus sawdust using $NaClO_2$, NaOH and KOH.	Yield ˜80 wt.%. Zeta potential (mV) -24 to -60	Ferreira, R.R. et al. [65]
Planetary ball mill	ITO LP-1 Planetary pot mill,	milling speed of 400 rpm for 2 h	cellulose powder	Crystal size 2-4 nm, degradation 220–410 °C with thermal decomposition peak at 373 °C with 80 wt% loss	Phanthong, P. et al. [94]
Planetary ball mill	XQM-0.4A, Tencan powder, Changsha, China)	speed of 400 rpm, 3 h in cycles of 20 min/milling per 10	Cellulose from pineapple peel	Nanofibrils size 19-24 nm, Zeta potential (mV) -22 to -28.	Wang, Y. et al. [60]

 doi:10.20944/preprints202602.0729.v1

		min/rest. NaOH-assisted.			
Planetary mill	Naraya-MPM-2 × 250H mill (Amin Asis Fanavar Pars), 250 mL jar, 60% stainless steel balls of 0.5–2 cm, 30% sample	speed 200 rpm for 2 h. dispersed in deionized water prior ultrasonic-assisted,	Cellulose from Cuminum cyminum waste	Zeta potential (mV) -25. Size 25 nm. degradation peak around 330 °C	Hoseinpour, Z. et al. [66]
Tumbler Ball Mill	impact ball mill (MA500, Marconi Ltda., Piracicaba, SP, Brazil)	alumina balls (diameter of 21 mm), 70 g of alumina balls for 1 g of cellulose fiber. Time 6, 9, and 12 h. ethanol-assisted	Cellulose from corn stalks, cobs, and husks	Zeta potential (mV) -15 to -41 (stalk), -13 to -42 (husk), -30 to -38 (comb). Size 70-195 nm	dos Santos, D.F. et al. [62]

5. Characterization of Nanoparticles

The particle size and dimensions, and shape are some of the factors that can influence the end-user properties of nanocellulose such surface charge, crystallinity, and thermal stability.

5.1. Surface Charge

Zeta potential (ζ-potential) expressed in modulus, is a surface charge and a key primary parameter that measures the electric charge on the surface of nanoparticles when dispersed in aqueous medium, and in most part controlling the rheological behaviour [63]. The surface charge can be ascribed to protonation and deprotonation on the particle surface, and formation of electric double layer [64]. It is an indicator of electrostatic repulsion between particles and for predicting the stability of nanoparticles and colloidal behaviour. The zeta potential for nanoparticles from cellulose were reported in the range -16 mV to -60 mV [59, 65, 66]. The stability behaviour of nanocellulose in suspensions can be classified as stable for modulus $\zeta > 30$ mV. In this range, surface charge prevents aggregation of the particles. The suspensions with modulus $\zeta < 15$ mV are described as highly unstable and can exhibit rapid coagulation. The suspensions $\zeta \sim 20$ mV can show initial stability with gradual aggregation of particles. Other reports showed that nanoparticles with a ζ between -10 and +10mV are considered neutral. The differences in the reported data on zeta potential can be ascribed to particle size. The smaller particles are likely to register higher surface charge density and thus higher modulus zeta potential [67]. The aqueous solution with higher electrostatic repulsion showed less aggregation and greater colloidal stability [68], and was dependent on particle size, composition and pH of the medium [69]. The development and modification of nanomaterials are aimed at colloidal stability by avoiding aggregation of particles and achieving high modulus values of zeta potential. The zeta potential can be measured using Zetasizer Nano-ZS (Malvern Panalytical Ltd., Malvern, U.K.), a common instrument based on principles of electrophoretic mobility of particles [65]. For computing ζ, the velocity at which particles move toward a positive electrode is measured 15-16 times repetitions at specified time such as 10s for each trial [59, 65, 66].

5.2. Particle Size and Shape

Based on size and dimension of the particle, the classification of nanomaterials is tabulated in Table 4. The dimensions are confined to the nanoscale size in the range 1 – 100 nm in which the nanomaterials are classified into four categories: zero-dimensional, one-dimensional, two-dimensional, and three-dimensional, abbreviated as 0D, 1D, 2D, and 3D, respectively. The 0D has three dimensions (length, width, height) within the nanoscale. When one dimension is > 100 nm, the particle is referred to as 1D nanomaterials. The 2D nanomaterial has two dimensions > 100 nm. The 3D particle has three dimensions > 100 nm. In these measurement, thickness or thinness of the particle is considered as diameter. There is no known nanocellulose material that were reported to exist in the range of zero-dimensional material. The nanocellulose particle size were reported in the range of

 doi:10.20944/preprints202602.0729.v1

2 - 450 nm (Table). Although reported data described particle >100 nm as nanoparticle, it is worth noting that nanoparticles should fall in the category <100 nm. The nanocrystals and nanofibrils exhibited particle less than 4 and 30 nm, respectively, and different morphologies. The transmission electron microscopy showed that nanofibers were fibrils, filamentous-like in shape, while nanocrystals showed rigid and rod-like structures. The variations in shape and size can be ascribed to differences in ball milling speed and time. The longer milling time led to insignificant differences in particle size, and yielded the lowest nanocrystals size [70]. The ball milling assisted processes including wet milling of both water and chemical agents, and ultrasonication yield smaller nanoscale particle than dry milling and unassisted milling [71]. The particle size distribution and average particle size of nanoscale can be analysed using Zetasizer Nano S90 apparatus (Malvern Instruments, UK), which operates based on laser beam scattering technique.

Table 4. Nanoparticle dimensions.

Dimension	Nanoscale	Shape	Nanomaterials	Reference
Zero dimension (0D)	Dimensions length, breadth, height (x,y,z) < 100 nm	Spherical, quasi-sphere, cubic, polygonal	Carbon dots, fullerene, clusters, grains, nanoparticles	Paras et al. [147]
One dimensional (1D)	Two dimensions (x,y) < 100 nm, and third dimension (z) >100 nm	needle-like	linear structures, carbon nanotubes, metals or metal oxides nanowires, polymer nanowires, nanofibers, hybrid materials	Su, B. et al. [148]
Two dimensional (2D)	One dimension (x) <100 nm, other two dimensions (y,z) undefined	atomically thin sheets, sheet-like honeycomb	Nanofilms, nanolayers, and nanocoatings	Li, X. and Wang, J. [149]
Three-dimensional (3D)	Dimensions (x,y,z) > 100 nm, not confined to the nanoscale.	Nano-cubes, fullerenes, dendrimers, and nanocages	Cellulose Nanocrystals (CNCs) and Nanofibrils (CNFs)	Dutta, S. et al. [150]

5.3. Surface Area

The catalysing effect of nanomaterial are in function of surface area. The surface area of nanomaterials from waste biomass were shown in the range 110-2060 $m^2 g^{-1}$ (Table 2). The lowest and highest surface area were reported in nanocellulose and graphene, respectively. The variation in surface area could be ascribed to differences in activation processes. During pyrolysis, the lignocellulose components (hemicellulose, cellulose, and lignin) are thermally decomposed, and volatiles (gas, tar) escape leading to the formation of micropores in the resulting product of solid carbon. Du Plessis, M. [72], demonstrated that surface area was inversely related to pore diameter of nanomaterial; and porosities of <50 µm formed interconnected biomaterials. The micropores (<2 nm) and mesopores (2–50 nm) can contribute significantly to the total surface area of bionanomaterials. The ball milling of solid carbon (biochar) can create the micropores (<2 nm) within the carbon matrix as graphene-like sheets are formed and rearranged. The thermal decomposition temperatures can reorganize the carbon atoms into disordered nanocarbons (graphene-like sheets) leading to increased surface area. The source and composition of waste biomass can influence the surface area of nanomaterials. The pyrolysis of wood materials with higher lignocellulosic contents were shown to produce nanocarbons with higher surface area. The presence of silica and alkali salts in grasses and straws can limit the surface area by promoting particle aggregation through the formation of formation of Si-O-Si bonds [73]. Similarly, materials with high ash content such as manure were associated with low surface area. High ash content can promote particle size agglomeration [74], and signified ash as parameter for selection of cellulose for suitability of producing nanoparticles. Higher percentage of ash in biomass would suggest less cellulose content. The microfibrillation significantly increases the specific surface area of nanocellulose. The combination of ball milling with assisted technology such as high-pressure homogenization can breakdown the cellulose fibres resulting into

 doi:10.20944/preprints202602.0729.v1

individual nanofibers or nanofibril, which are flexible and can form highly entangled network with many exposed surfaces [75]. The oxidation of nanofibrils can increase the surface area. The 2,2,6,6-tetramethylpiperidine1-oxyl (TEMPO)-oxidized cellulose nanofibrils exhibited an increase in surface area. The TEMPO oxidation process introduces negatively charged carboxylate groups on the surface of the cellulose microfibrils. The gas sorption analysis using nitrogen as carrier (Brunauer-Emmett-Teller Method) to generate N_2 adsorption/desorption isotherms is the common method of measuring surface area of dry nanocellulose powders [76]. Other methods included open-cell tetrakaidekahedron method specifically measuring surface area of bacterial nanocellulose. In this method, the biological activity of a scaffold depends on its surface area per unit volume, and the specific surface area was associated with pore size and the relative density [77].

5.4. Morphologies of Nanocellulose

The different types of nanocellulose such as nanofibrils and nanocrystals can exhibit a variation of morphologies (size and shape) based on the origin of nanomaterial, extraction method, and activation processes. The acid hydrolysis can breakdown and remove the amorphous region of cellulose to generate cellulose nanocrystals with rod-like and whisker-shaped, and rigid structures. The remove of amorphous increases crystallinity [78]. The rod-like shapes can measure 3-50 nm in diameter, and length of 50-500 nm with aspect ratio approximately 5-50. However, the treatment time and acid concentration can influence the size of particles. Rana, M.S. et al. [79], demonstrated that increased concentration and reaction time of sulfuric acid on cellulose resulted in particle size reduction from 800 nm to 600 nm, at 20 min and 45 min treatment time, respectively. Nevertheless, increased reaction time decreased the yield of cellulose nanocrystals by approximately 10%. The exposure to high concentration of acid at longer time can degrade the amorphous region, and this probably can explain the resulting smaller grain length of cellulose nanocrystals. The cellulose nanofibrils showed, long fibrillar network, flexible and entangled web-like structure. The mechanical processes combined with assisted technologies including high-pressure homogenization and pre-treatment of enzymatic or chemical nature, are a series of processes for transformation of cellulose into cellulose nanofibrils with intact crystalline and amorphous regions [80]. The individualized cellulose nanofibrils exhibited diameter of 3-5 nm and the length of 100-2000 nm. The surface topography including shape and size can be examined and measured using scanning electron microscopy [73], atomic force microscopy (AFM) and transmission electron microscopy (TEM) [81]. These techniques are limited on measuring the length of highly entangled networks of nanofibrils and non-spherical nanomaterials. To overcome this challenge, the microscopy techniques are integrated or combined with other software techniques to facilitate measurement of length, diameter or width. The microscopy image outputs can be processed using ImageJ software [82] or DiameterJ software [83] to determine the size of nanocellulose particles [84]. The sample suspensions of nanofibers and nanocrystals were examined using dynamic light scattering (DLS) and field-emission scanning electron microscopy (FE-SEM) [85]. The DLS can measure diameter of spherical nanoparticles having same diffusion coefficient in water. Thus, in the work of Tarrés, Q. et al. [85], DSL was applied to estimate hydrodynamic diameter of rod-like cellulose nanoparticles for assays where the scatter angle and the consistency were uniform. The use of forward scattering angle, and varying the concentrations are some of the recommendations for assays with different scatter angles. The FE-SEM determined the diameter of the nanofiber bundles, and the length of fibrils was estimated using geometrical relations [85]. The sedimentation and agglomeration of particles hinder measurement of dimensions, and such limitations can be addressed by increasing polydispersity using appropriate concentrations within the range of 0.05-0.75 wt%. Depending on analytical technique, concentrations of >1 wt% are possible. The combination of DSL and Field emission scanning electron microscopy and Transmission electron microscopy (FE-SEM and TEM) was used on colloidal solution of 2 wt% nanocellulose [65].

 doi:10.20944/preprints202602.0729.v1

5.5. Crystallinity

The molecular structure of elemental cellulose contains fibril units bound together through hydrogen bonds between the OH^- groups of the anhydroglucose molecules in the chain. These fibril units comprise of two structural domains, which are crystalline and amorphous. The crystalline domain is well ordered molecular structure while amorphous is structurally disordered [86]. The elemental fibrils can bundle together through hydrogen bonding to form nanostructure called microfibrils also known as nanocellulose (or nanofibrous material). The hydrogen bonding can exhibit specific geometric arrangements of atoms through covalent bonds and electrostatic attractions, creating different structure configuration and molecular orientation, often linear but also complex networks like rings or chains (dimers, trimers) in liquids and solids. Accordingly, the variation in configuration can yield different material properties. Based on hydrogen configuration, and molecular packing and orientation, cellulose is classified into different crystalline structures called polymorphs (I, II, III, IV) [87]. The polymorphs are characterized using unit cell lattice parameters of the six fundamental dimensions (three edge lengths: a, b, c, and three interaxial angles: α, β, γ) that are used to define the size, shape, and orientation of the smallest repeating unit (fibril) in a crystal structure, allowing the construction of the entire crystal lattice [88]. The orientation or chain configuration can be described as parallel or antiparallel in function of edge lengths and interaxial angles. Cellulose I naturally occurring crystalline structure of fibrous material, was reported to have two substructures namely cellulose I_α and I_β [88]. These polymorphs are described as parallel chain configuration based on I_α lattice parameters of length: a (0.672 nm), b (0.596 nm) and c (1.040 nm) and interaxial angles: α (118.08°), β (114.80°) and γ (80.38°) while I_β lattice parameters of length: a (0.778 nm), b (0.820 nm) and c (1.038 nm), and interaxial angles of α (90°), β (90°) and γ (96.50°). The variations in chain configurations can be assigned to differences in the source of cellulose, extraction method and treatment methods.

The relative amount of crystalline and amorphous in a given cellulose sample can be described by crystallinity index. The X-ray diffraction (XRD) is the common technique of measuring the degree of crystallinity index. The common operation in most of XRD techniques is the Cu Kα (Copper K-alpha) radiation with characteristic X-ray wavelength (around 1.54 Å or 0.154 nm) and can be generated using voltage of 40 kV and amperes of 40 mA (Table 5) at angular positions of 2θ (2theta) in the range of 2–70°. The data output from XRD is X-ray diffraction spectra and can be analysed using Segal method to calculate percentage crystallinity index [88, 89]. The XRD spectra can be used as criteria for the selection of fibre materials for suitability of processing nanocellulose. The percentage crystallinity of cellulose was reported in the range of 20-88%, and varied according to chemical composition, extraction method and treatments. The XRD spectra for raw rice husk and keya leaf showed several XRD peaks at various 2θ positions (Table 5). The peaks are indicative of the distinct lattice planes of fibrous structure, and spectra with several peaks is a sign of cellulose I, a native fibrous material rich in lignocellulose contents. The chemical treatments such as alkalinisation and bleaching of cellulose I (i-e. raw agricultural waste) can degrade amorphous region and subsequent removal of hemicellulose and lignin, and thus these treatments eliminate other peaks resulting in a single peak and the rise in the crystallinity index. This progressive elimination of peaks can be a quality criterion for successful production of nanocellulose and nanocellulose crystals. The source of cellulose can influence crystallinity index. The crystallinity index (40-56%) of raw rice husk varied according to the rice variety [90]. This suggested that specific source of plant can determines genetic structure of the cellulose including the ratio of its crystalline to amorphous regions. Nonetheless, there are limited studies that demonstrated crystallinity index as a function of genetic factors such as plant germplasm of the waste biomass. The variation in crystallinity index according XRD technique and operation inputs were shown to be insignificant (Table 5). This implied that different XRD techniques and specific operational procedures such as sample preparation or data analysis methods like Sego method yielded consistent and non-varying results.

 doi:10.20944/preprints202602.0729.v1

Table 5. Crystallinity of nanocellulose.

Nanoparticles	Source of Waste Biomass	Technique	Crystalline Properties	Reference
Cellulose nanofibrils	Pineapples peel	XRD (X'Pert3 Powder, Malvern Panalytical, Almelo, The Netherlands)	Crl 38-44%, Crystal size (D) 2-3 nm	Wang, Y. et al. [60]
Nanocellulose	Cumin husk	XRD, Karlsruhe instrument (Germany), input: CuKα radiation (λ = 0.1542 nm, 40 kV, 40 mA). Position: 2θ range of 5–65°, scan rate of 3°/min	XRD peaks at 2θ =18° and 22.6° Clr 69.3% at 2θ=22.6° Crystal size 3.76 nm	Hoseinpour, Z. et al. [66]
Nanocellulose	Maguey fibre	XRD, LabX-6000, SHIMADZU, Japan. Input: 40.0 kV and 30.0 mA with Cu Kα radiation (1.5148 Å). 2θ range of 2-70°, scan speed 1°/min	XRD peaks ~ 2θ = 15.52° and 22.64°, Crl 74.80% at 2θ=22.64°	Sumarago, E.C. et al. [151]
Raw fibre	Keya leaf (alkali and bleach treatment)	Wider angle XRD, BRUKER D8 ADVANCE, input: Cu Kα radiation (α = 0.154 nm) at 40 mA and 50 kV.	Raw fibre Crl 45.35% at 2θ = 14.79°, 22.59°, 24.25°, and 29.97. Alkali fibre Crl 54.69% at 2θ=22.97° Bleached fibre Crl 43.43% at 2θ=22.8°	Hossain, M.I. et al. [152]
Nanocellulose crystals	Keya leaf	Wider angle XRD, BRUKER D8 ADVANCE, input: Cu Kα radiation (α = 0.154 nm) at 40 mA and 50 kV.	Clr 61.31% at 2θ=19.9° and 22.44°	Hossain, M.I. et al. [152]
Nanocellulose crystals	Peanut shells	XRD, RIGAKU MINIFLEX-600 input: Cu Kα (λ=1.54 A0), scanning in a 2θ range of 10-50°	Crl 26-66% at 2θ=22.6°	Punnadiyil, R.K. et al. [153]
Nanocrystalline cellulose	Banana fibre	XRD, Shimadzu XRD-6000. Input: voltage of 30 kV and current of 30 mA, 2θ=5-60°, scan rate 2 °C/min.	XRD peaks at 2θ = 16.1°, 22.8° and 34.9° Crl 62% at 2θ = 19 and 22.2°	Mishra, S. et al. [154]
Nanocellulose	Rice husks (variety)	XRD, MiniFlex 600 (Rigaku, Japan). Input: Cu Kα λ = 1.54, acceleration potential =40 kV, current = 15 mA. scan range of 2θ = 2-60°, scan rate 3°/min	XRD peaks 2θ = 16.3°, 22.4° and 34.5° for raw husk. Crl for husk 40-56% at 2θ=22.4° Crl for cellulose 46-66% at 2θ=22.4° Crl for nanocellulose 59-77% at 2θ=22.4°	Rashid, S. and Dutta, H. [90]

Crl=Crystallinity, 2θ=Theta Position.

5.6. Thermal Properties

The thermal stability is the most desired thermal characteristic, an indicator of the temperature at which the cellulose and nanocellulose material can thermally decompose. In most part of literature, the thermal decomposition temperature of nanocellulose was reported in the range 150 – 350°C (Table 5). Some of the factors that can explain the variation are source of nanomaterials, extraction method, and surface chemistry including contents of lignin and hemicellulose. The molecular crystal structure of nanofibrous can also influence the process of thermal decomposition of the cellulose. The nanocrystals derived from the process of acid hydrolysis, have the amorphous parts of cellulose degraded by the acid molecules, on the other hand, the crystalline region of cellulose is resistant to the acid and remained undegraded. The high crystallinity index (80-90%) of cellulose nanocrystals were shown to correlate positively with higher thermal stability and decomposition temperatures [91]. The thermogravimetric analysis (TGA) is the common non-destructive technique for generating thermal profiles on thermal properties, structure and performance of cellulose and derived cellulose materials aimed at possible high-temperatures applications. In the TGA method, the samples are heated in the temperature range of 20 - 600 °C at constant heating rate of 20°C min^{-1} under nitrogen gas flow using an instrument STA 6000 (PerkinElmer, USA). The generated graphs can be analysed using software packages such as OriginPro software [92]. The thermogravimetric graphs are plotted

 doi:10.20944/preprints202602.0729.v1

as weight% in function of heating temperatures. Hoseinpour, Z. et al. [66], showed that derivative thermogravimetry data exhibited three stage thermal curves of nanocellulose processed from cumin husk. The first curve was associated with endothermic peak temperature required for initial weight loss as a result of drying due to evaporation of bound water molecules and volatile compounds. This stage has slower degradation rate due to the higher thermal resistance of more ordered cellulose components. The second curve showed onset degradation temperature for degradation of hemicellulose and breakdown of some parts of amorphous cellulose. In this stage, the peak degradation temperature (Tmax) is indicative of depolymerization of cellulose into volatile products, primarily anhydro-saccharides such as levoglucosan, and initial formation of char, gases (carbon dioxide and water vapour), and volatile organics. The third stage was associated with thermal decomposition of the remaining parts of amorphous and crystalline cellulose leading to volatilization and complete formation of char structures. The thermal decomposition of fibre and nanocellulose derived from bamboo exhibited similar weight loss profiles at the initial drying stage and peak decomposition temperatures [93]. However, the final decomposition showed higher weight loss of up to 15 wt% in nanocellulose than those in fibre (12 wt%). The nanocellulose exhibited higher residue weight loss and lower decomposition temperature than those of cellulose [94]. The surface area can explain these observations. The nanocellulose has higher surface area with less impurities, and hence lower resistance against heat transfer. The high surface area was negatively correlated with thermal stability, suggesting that as the surface area increases, the nanomaterial becomes highly susceptible to thermal decomposition [95]. Although, nanocellulose has higher crystallinity than that of cellulose, the factors associated with the "nano" scale and extraction process can contribute to the reduction of its thermal stability. The process of producing cellulose nanocrystals using sulfuric acid hydrolysis can modify the particles by introducing sulphate groups on the surface. The interaction of sulphate groups with hydroxyls can release water molecules. This water can lower both the onset temperatures and activation energies of cellulose pyrolysis. The acid hydrolysis can enhance the breakdown of the β(1→4) glycosidic bonds of the cellulose chains leading to increased production of reducing ends or terminal ends of cellulose. This can lead to decreased degree of polymerization. The decreased degree of polymerisation and increased number of reducing ends can account for lowering of onset temperature. The sulphate increases formation of charred residue which act as flame retardant, and this can also decrease the onset temperature.

Table 6. Thermal properties of nanomaterial.

Nanoparticles	Source of Biomass	Technique	Thermal Properties	Reference
Cellulose	Eucalyptus saw dust	TGA, heat 20 - 600°C. instrument: STA 6000 (PerkinElmer, USA	T_{max} 367°C	Ferreira, R.R. et al. [65]
Nano cellulose	Eucalyptus saw dust	TGA, heat 20 - 600 °C. instrument: STA 6000 (PerkinElmer, USA)	T_{maz} 321-342°	Ferreira, R.R. et al. [65]
Nanocellulose	Cumin husk	TGA, 20 – 600°C, heat rate 20°C/min, STA 6000 (PerkinElmer, USA)	Initial weight loss (50-150°C), T_{max} (275–365°C), thermal decomposition (>400°C)	Hoseinpour, Z. et al. [66]
Extracted fibre	Bamboo	Thermal Analyzer, temp 40 - 700°C, Hitachi STA 7300, heating rate of 10°C/min. Sample weight (3-5 mg).	minor weight 5-7% (100-300° C), major weight loss 40-41% at peak decomposition (300-400°C), final weight loss 10-12% at final decomposition (>350°C)	Verma, Y.K. et al. [93]
Nanocellulose	Bamboo	Thermal Analyzer, temp 40 - 700°C, Hitachi STA 7300, heating rate of 10°C/min. Sample weight (3-5 mg).	minor weight 5-6% (100-300° C), major weight loss 40-41% at peak decomposition (300-400°C), final weight loss 10-15% at final decomposition (>350°C)	Verma, Y.K. et al. [93]
Cellulose	Cellulose paper	TGA, thermal Analyzer (DTG-60H, Shimadzu), temp 20 - 600°C, Heating rate 10°C/min	major degradation temp (370°C), weight loss (87%) and residue weight loss (6%) at 600°C.	Phanthong, P. et al. [94]

 doi:10.20944/preprints202602.0729.v1

Nanocellulose	Cellulose paper	TGA, thermal Analyzer (DTG-60H, Shimadzu), temp 20 - 600°C, Heating rate 10°C/min	major degradation temp (200-420°C), weight loss (75%), max decomposition temp (340-350°C). residue weight loss (15%) at 600°C.	Phanthong, P. et al. [94]
Fibrous	Pineapple pee (hot, bleach and alkali treated)	TGA, thermal analyser (TGA550, TA Instruments, New Castle, DE, USA), temp 30 – 600° C, heating rate 10°C/min	Onset temp (220-240°C) and max temp (340-345°C), char residue (5-19%).	Wang, Y. et al. [60]
Cellulose nanofibrils	Pineapple peel	TGA, thermal analyser (TGA550, TA Instruments, New Castle, DE, USA), temp 30 – 600° C, heating rate 10°C/min	Onset temp (230-245°C) and max temp (316-330°C), char residue (14-17%).	Wang, Y. et al. [60]

6. Rheology Behaviour of Nanocellulose

The study of rheology properties of nanocellulose are aimed at understanding the impact of force on flow and deformation behaviour of nanocellulose in dispersions and suspensions. The flow or deformation behaviour can technologically define suitability of nanocellulose for processing. In practice, rheology relates to mixing properties of nanocellulose when included as additive (nanofiller) and ingredient in suspensions (fluids). The suspensions are plasticizers such water, glycerol and sorbitol [96], to mention just a few common examples. The role of plasticizer is to raise plasticity, workability, and swelling capacity through disruption of intermolecular forces and generate mobility of the polymer chains [97, 98]. The disruptor is the applied force or torque (shear stress). The nanocellulose and cellulose suspensions were reported to exhibit non-Newtonian fluids, expressing properties like high viscosity and gel-like structures at low shear rates. The viscous or gel-like structure can be dominated with formation structural network through hydrogen bonding, entanglement and electrostatic interactions of chains. Depending on rheological behaviour, cellulose, nanocellulose and nanofibrils can find industrial application in coatings, food additives, cosmetics, 3D printing, and as rheology modifiers [99]. The network of nanocellulose can exhibit solid-like gel or flocculated structure, behaviour characteristic of yield stress, high viscosity and viscoelastic at resting state (without external force). The yield stress is associated with nanocellulose behaving like solid and sustains its shape until the external force (stress) is greater than specific threshold. The viscoelasticity behavior relates to elastic properties, soft solid or gel with ability to recover after small deformation. The external force when applied, can break down the network (solid-like gel) of nanocellulose into shear-thinning, the state of deformation and flowing like liquid [99]. The external force generates shear stress due to stirring, shaking, or pumping of cellulose or nanocellulose suspensions [100].

The nanocellulose, cellulose nanofibrils and cellulose nanocrystals act as nanofillers, influencing mechanical properties of biocomposites made from biodegradable polymer matrices such as starch. The biocomposites can be processed using melt compounding, extrusion, injection molding, solvent casting, and 3D printing [101], and these processes are governed by rheology (mixing properties). In view of this, rheology properties find use in process control and systems analysis, and design of piping technology.

The interaction between nanocellulose and starch or other base matrix polymers can increase viscosity by developing a network of hydrogen bonding and structural entanglement. This interaction can limit polymer chain mobility resulting in elevated viscosity. The addition of 1-5 wt.% cellulose nanocrystals into thermoplastic starch decreased the melt flow index from 2.10 g/10 min to 1.40 g/10 min [102]. Similarly, the inclusion of cellulose nanocrystals into polylactic acid films composite suspensions resulted into increased viscosity [103]. This suggested increased molecular weight retention, indicative of increased formation of hydrogen bonding between ester and hydroxyl groups, and entanglement in coated samples. The cellulose nanocrystals have high aspect ratio and rigid structure which creates chain entanglement resulting in increased hydrodynamic volume setting up resistance against flow of composite suspension [104, 105]. The percentage inclusion of cellulose nanocrystals >3-5% by weight was reported to build agglomeration in suspension, and can

 doi:10.20944/preprints202602.0729.v1

influence negatively the mechanical properties of polylactic. Such nanocellulose dispersions exhibited minimum yield stress to initiate the flow. This shows that below minimum stress; the composite remains in the state of gel (soft solid behavior). In fact, this is a vital behavior for stabilizing dispersions or suspensions of gel nature in paint and food industry. The application of force greater than stress yield can cause internal structure deformation resulting in increased molecular mobility leading to the flow of the suspension. This effect is called shear-thinning (pseudoplasticity), and is the desired state for casting, spraying and melt flow, and compression processes. The rheology properties can be characterized using torque rheometers [106] to generate shear stress-shear rate (γ°) curves or viscosity (η)-shear rate (γ°) curves. Rheological properties such as storage modulus (G′), loss modulus (G″) and complex viscosity (η) are key parameters for describing the flowability and flow nature of the composites. The G' and G'' are measured when strain (shear rate) is applied [107]. The flow behaviors are characterized using rheology models such as Herschel-Bulkley [108, 109], Power Law [110] and Bingham Plastic [109]. The curves (Fig. 1) can describe the nature of flow of polymeric composite solution. The gel structure with G' > G'', is indicative of a solid-dominant material. Both G′ and G″ correlated positively with the increasing loading of cellulose nanocrystals into nanocellulose composites [103]. This is indicative of composite exhibiting increasing stiffness and viscosity with higher energy dissipation. This behavior is a good example of dilatant fluids (Figure 1) showing shear thickening properties such as increase in viscosity with the rate of applied shear stress. For example, the behavior of starch in water. The Pseudoplastic (thinning properties) was illustrated [107].

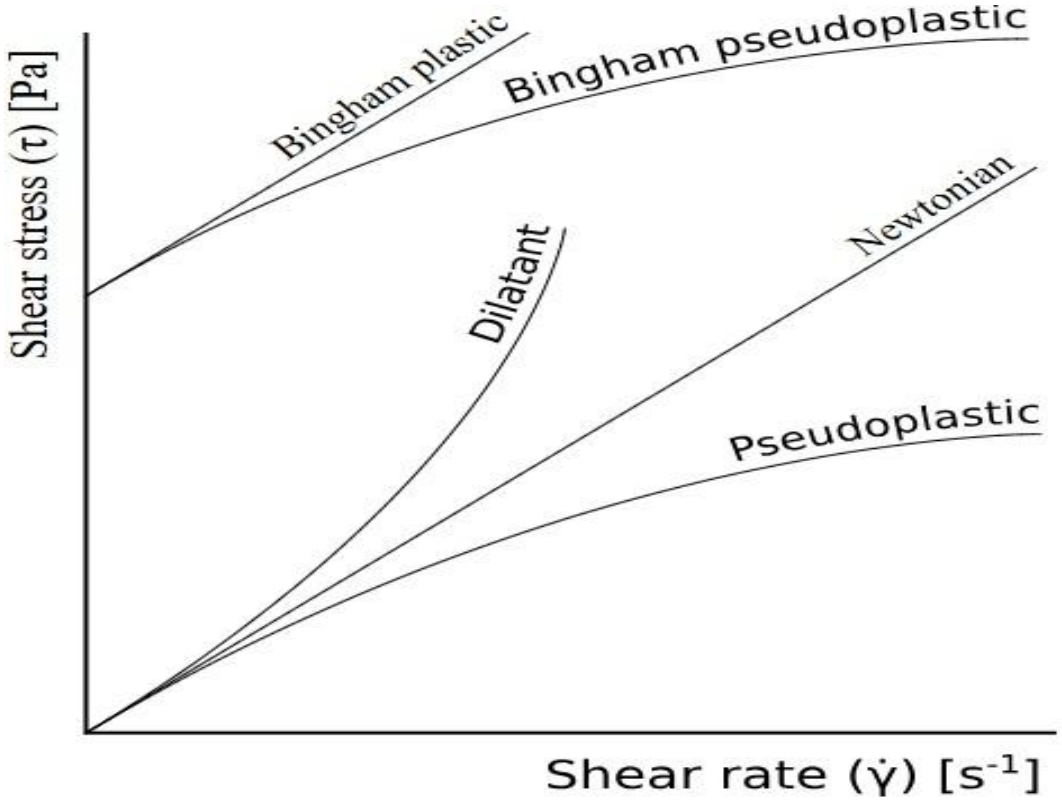

Figure 1. Example of stress-strain curves for non-Newtonian dispersions or suspensions. Source: Wikipedia.

7. Application of Cellulose-Derived Nanoparticles

The nanoparticles such nanocellulose, nanocrystals and biochar particles can be used as ingredients, additives and nanofillers in production of biocomposites. The of functionality of nanoparticles in biocomposites is in function of thermal stability, capacity to form H-, C-C bonding

 doi:10.20944/preprints202602.0729.v1

and entanglement with polymer matrices. Additionally, rheology is the key quality criterial for deciding the usefulness of nanoparticles in viscous flow technologies.

7.1. Packaging

Nanocellulose serves as additives or ingredients in production of high-barrier packaging films. The Poly-(butylene succinate), a biodegradable polymer matrix, was coated and laminated using layered spray-coating technique at ~0.4% nanofibrillated cellulose of the bio-composite weight [111]. The resulting film decreased water vapor transmission rate by approximately 6-fold. Additionally, optical transparency of the laminates showed a significant drop 70-30% of the visible light spectrum [111]. The nanocellulose can create excellent oxygen barriers, protecting food from oxidation. The mixture of Polyvinyl alcohol/cellulose nanofibrils supplemented with iron ions, yielded a composite film that showed a decrease of oxygen transmission rate of approximately 70% [112, 113]. The ingredient Iron (Fe^{3+}) enhanced bonding by improving crosslinking and interaction of carboxyl with hydroxyl groups. Edible coating loaded with nanocellulose yielded antibacterial surface on strawberries resulting in extended shelf life [114, 115]. The high surface area and charge of nanocellulose heightens interaction of nanocellulose with bacterial cell membrane, increasing interference with DNA/proteins, which probably can disrupt bacterial biofilms. Nanocellulose can act as carrier of antibacterial agents.

The cellulose nanocrystal was mixed with silver nanoparticles to prepare nanocomposite ingredient for production and fabrication of antibacterial paper [116]. Nanocellulose can find application in processing of foams & cushioning products. The cellulose nanofibrils facilitated production of ultra-lightweight aerogels and foam products with improved ductility and thermal insulation with great thickness recovery [117]. The nanostructured salinized cellulose nanofibrous frameworks generated a 3D nanoporous structure and exhibited silica aerogel materials of lightweight with insulating capacity of ultralow thermal conductivity of around 15.9 mW m^{-1} K^{-1} [117]. The biochar impregnated with silver nanoparticles (ZnO, Zn) showed suitability for development of active packaging materials by exhibiting an excellent combination framework of good electrical conductivity (6.7×10^{-4} S m^{-1}), higher antioxidant potential with inhibition capacity of > 8 h, and higher antibacterial activity against bacterial pathogens [118, 119].

7.2. Rheology Modifiers and Thickeners

The cellulose nanofibrils can form pseudoplastic fluid, a shear-thinning gel in water at low concentrations of the range 0.1-2% wt. This implied that under shear-thinning, the cellulose nanofibrils can quickly cause decrease in viscosity of gel, and can rapidly restore gel viscosity when stress is released [120]. This rheological property makes cellulose nanofibrils a good ingredient candidate in the food industry for the production of stabilizers for application in sauces, creams, ice cream, and whipped toppings, replacing fats or synthetic thickeners. The cellulose nanofibrils was used as aqueous phase in the preparation of oil-in-water Pickering emulsion, the process of which resulted in an emulsion with increased zeta potential and viscosity, indicative of improved stability of the emulsions [121]. The emulsion instability associated with the use of native nanocellulose was addressed by preparing cellulose nanofibrils with high carboxyl content using sodium periodate and TEMPO two-step oxidation process to produce Pickering emulsions using assisted-technology of ultrasonic emulsification and high-pressure homogenization. The resulting fabricated carboxyl-cellulose nanofibrils showed excellent stability with creaming index of the emulsion of more than three months under storage conditions of low temperature 4 °C [122]. Inclusion of cellulose and cellulose nanofibers into shear stiffening gel resulted in composite structural framework of cellulose-supported stiffening gel and CNF-supported stiffening gel, with peak storage modulus of 908 MPa and 15.3 MPa, respectively. These properties inhibited the cold flow deformation of stiffening gel and showed enhanced impact-resistant performance [123]. Nanocellulose derived from *Ulva lactuca* (sea lettuce) was blended with fluoride and tested for antibacterial activity against *Streptococcus*

 doi:10.20944/preprints202602.0729.v1

mutans and *Lactobacillus acidophilus* [124]. The resulting composite exhibited higher inhibition capacity against the pathogens making it antimicrobial agent for application in tooth paste [124].

8. Conclusions

The percentage crystallinity and cellulose content are principal selection criteria of agricultural waste biomass for production of nanocellulose and nanofibrils, and including biochar-derived nanocarbons. The properties such as composition, surface charge, surface area, zeta potential, morphology, and thermal decomposition temperatures can vary according to diversity in crop types and extraction methods. Moreover, particle size and dimensions, and shape are some of the factors that can influence the end-user properties of nanocellulose. Pyrosis is eminently the strategy for transformation of agricultural waste into biochar-derived nanoparticles, and yet there are limited studies on landfills into biochar for useful industrial applications.

Author Contributions: Conceptualization, SMC.; methodology, SMS, ZS; investigation, resources, SMC, FCM.; data curation, SMS, OMO; writing—original draft preparation, SMC; writing—review and editing, SMC; visualization, supervision, JY, AMM, PK; project administration, JY, HL, FCM; funding acquisition HL, FCM. All authors have read and agreed to the published version of the manuscript.

Funding: This work was funded and supported by The Royal Society (UK) International Collaboration Awards 2024 (Brazil and South Africa) - ICAO\R1\241143.

Data Availability Statement: Not applicable.

Conflicts of Interest: The authors declare no conflicts of interest.

References

1. Imma, P. *Bioactives from agricultural food by-products: application in food and health*. **2017**,
2. Nargotra, P., A. Yadav, D. Sharma, M.-L. Tsai, B.K. Bajaj, V. Sharma, *Integrated technologies for agro-waste valorization*, in *Agriculture-Bioenergy Nexus*. 2026, Elsevier. p. 351-385.
3. Mikus, M.,S. Galus, *Biopolymers from agriculture waste and by-products*, in *Biopolymers: Recent Updates, Challenges and Opportunities*. 2022, Springer. p. 111-128.
4. Phiri, R., S.M. Rangappa, S. Siengchin, O.P. Oladijo, H.N. Dhakal. *Development of sustainable biopolymer-based composites for lightweight applications from agricultural waste biomass: A review*. *Adv. Ind. Eng. Polym. Res.* **2023**, 6, 436-450.
5. Choudhary, R., A. Kumar, V. Kumar, M.H. Elmnifi, S. Dhar, F.M. Alqahtani, D. Sharma, C. Mahata, S.K. Chaudhari, S. Kumari, *Case study on biopolymers derived from food and agro-industrial wastes*, in *Food and Agro-Industrial Wastes*. 2026, Elsevier. p. 439-454.
6. Teli, M.,A.C. Jadhav. *Extraction and characterization of novel lignocellulosic fibre*. *J. Bionanosci.* **2016**, 10, 418-423.
7. Rencoret, J., G. Marques, M.J. Rosado, J. Benito, F. Barro, A. Gutiérrez, J.C. Del Rio. *Variations in the composition and structure of the lignins of oat (Avena sativa L.) straws according to variety and planting season*. *Int. J. Biol. Macromol.* **2023**, 242, 124811.
8. Lama-Muñoz, A., M. del Mar Contreras, F. Espínola, M. Moya, I. Romero, E. Castro. *Characterization of the lignocellulosic and sugars composition of different olive leaves cultivars*. *Food Chem.* **2020**, 329, 127153.
9. De, S., S. Mishra, E. Poonguzhali, M. Rajesh, K. Tamilarasan. *Fractionation and characterization of lignin from waste rice straw: Biomass surface chemical composition analysis*. *Int. J. Biol. Macromol.* **2020**, 145, 795-803.
10. Bhat, R., A. Ahmad, I. Jõudu, *Applications of lignin in the agri-food industry*, in *Lignin: Biosynthesis and transformation for industrial applications*. 2020, Springer. p. 275-298.
11. Vasile, C.,M. Baican. *Lignins as promising renewable biopolymers and bioactive compounds for high-performance materials*. *Polymers.* **2023**, 15, 3177.
12. Gautam, A., A. Kumar, A.K. Bharti, D. Dutt. *Rice straw fermentation by Schizophyllum commune ARC-11 to produce high level of xylanase for its application in pre-bleaching*. *J. Genet. Eng. & Biotechnol.* **2018**, 16, 693-701.

 doi:10.20944/preprints202602.0729.v1

13. Wu, W., P. Li, L. Huang, Y. Wei, J. Li, L. Zhang, Y. Jin. *The role of lignin structure on cellulase adsorption and enzymatic hydrolysis*. *Biomass* **2023**, 3, 96-107.
14. Xu, R., N. Doskaliuk, B. Pang, J. Xu, W. Xu, C. Xu, M. Antonietti, S. Filonenko. *Hemicellulose from mild extraction of biomass: Revealing structural insights and advancing potential value*. *Carbohydr. Polym. Technol. Appl.* **2025**, 100843.
15. Zhao, Y., H. Sun, B. Yang, Y. Weng. *Hemicellulose-based film: potential green films for food packaging*. *Polymers.* **2020**, 12, 1775.
16. Berg, J.M., J.L. Tymoczko, L. Stryer, *Biochemistry (loose-leaf)*. 2007: Macmillan.
17. Heinze, T., *Cellulose: structure and properties*, in *Cellulose chemistry and properties: fibers, nanocelluloses and advanced materials*. 2015, Springer. p. 1-52.
18. Tomisawa, R., M. Nagata, Y. Otsuka, T. Ikaga, K. Kim, Y. Ohkoshi, K. Okada, T. Kanaya, H. Katsuta. *Tensile strength of polyester fiber estimated by molecular-chain extension prior to structure formation*. *Sci. Rep.* **2023**, 13, 11759.
19. Glińska, K., J. Gitalt, E. Torrens, N. Plechkova, C. Bengoa. *Extraction of cellulose from corn stover using designed ionic liquids with improved reusing capabilities*. *Process Saf. Environ. Prot.* **2021**, 147, 181-191.
20. Freixo, R., F. Casanova, A.B. Ribeiro, C.F. Pereira, E.M. Costa, M.E. Pintado, Ó.L. Ramos. *Extraction methods and characterization of cellulose fractions from a sugarcane by-product for potential industry applications*. *Ind. Crop. Prod.* **2023**, 197, 116615.
21. Foroushani, M.Y., A.Y. Foroushani, H. Yarahmadi. *Analysis of mechanical techniques in extracting cellulose fibers from sugarcane bagasse*. *Biomass Convers. Biorefin.* **2025**, 1-14.
22. Rizwan, M., S.R. Gilani, A.I. Durrani, S. Naseem. *Cellulose extraction of Alstonia scholaris: A comparative study on efficiency of different bleaching reagents for its isolation and characterization*. *Int. J. Biol. Macromol.* **2021**, 191, 964-972.
23. Benali, M., A. Oulmekki, J. Toyir. *The impact of the alkali-bleaching treatment on the isolation of natural cellulosic fibers from Juncus Effesus L plant*. *Fiber Polym.* **2024**, 25, 525-533.
24. Zhang, M., X. Song, X. Sun, Z. Wang, Z. Li, H. Ji, X. Xu, J. Li. *The relationship between cellulose content and the contents of sugars and minerals during fiber development in colored cotton cultivars*. *Cellul.* **2012**, 19, 2003-2014.
25. Djahedi, C., L.A. Berglund, J. Wohlert. *Molecular deformation mechanisms in cellulose allomorphs and the role of hydrogen bonds*. *Carbohydr. Polym.* **2015**, 130, 175-182.
26. Baghaei, B.,M. Skrifvars. *All-cellulose composites: a review of recent studies on structure, properties and applications*. *MOL.* **2020**, 25, 2836.
27. Sousa, L.d.C., J. Humpula, V. Balan, B.E. Dale, S.P. Chundawat. *Impact of ammonia pretreatment conditions on the cellulose III allomorph ultrastructure and its enzymatic digestibility*. *ACS Sustain. Chem. Eng.* **2019**, 7, 14411-14424.
28. Chen, J., *Synthetic textile fibers: regenerated cellulose fibers*, in *Textiles and fashion*. 2015, Elsevier. p. 79-95.
29. Swatloski, R.P., S.K. Spear, J.D. Holbrey, R.D. Rogers. *Dissolution of cellose with ionic liquids*. *J. Am. Chem. Soc.* **2002**, 124, 4974-4975.
30. Lu, A., X. Yu, Q. Ji, L. Chen, A.E.-G. Yagoub, F. Olugbenga, C. Zhou. *Preparation and characterization of lignin-containing cellulose nanocrystals from peanut shells using a deep eutectic solvent containing lignin-derived phenol*. *Ind. Crop. Prod.* **2023**, 195, 116415.
31. Zhang, X., D. Bao, Y. Huang, H. Dong, X. Zhang, S. Zhang. *Gas–liquid mass-transfer properties in CO2 absorption system with ionic liquids*. *Am. Inst. Chem. Eng.* **2014**, 60, 2929-2939.
32. Andlar, M., T. Rezić, N. Marđetko, D. Kracher, R. Ludwig, B. Šantek. *Lignocellulose degradation: An overview of fungi and fungal enzymes involved in lignocellulose degradation*. *Eng. Life Sci.* **2018**, 18, 768-778.
33. Kumar, A.,R. Chandra. *Ligninolytic enzymes and its mechanisms for degradation of lignocellulosic waste in environment*. *Heliyon.* **2020**, 6,
34. Radotić, K.,M. Mićić, *Methods for extraction and purification of lignin and cellulose from plant tissues*, in *Sample preparation techniques for soil, plant, and animal samples*. 2016, Springer. p. 365-376.
35. Gonzalez-Gonzalez, M.d.R.,R. Miranda-Lopez. *Cellulases, hemicellulases and ligninolytic enzymes: mechanism of action, optimal processing conditions and obtaining value-added compounds in plant matrices*. *MOJ food process. technol.* **2022**, 10, 30-37.

 doi:10.20944/preprints202602.0729.v1

36. Sigma-Aldrich®. *Ilya Koltover, Ph. D. Aldrich® Materials Science Sigma-Aldrich® Corporation*.
37. Zhang, J., P. Li, Y. Yu, Y. Xu, W. Jia, S. Zhao. *A review of natural polysaccharides-based flocculants derived from waste: application efficiency, function mechanism, and development prospects*. *Ind. Eng. Chem. Res.* **2023**, 62, 15774-15789.
38. Zhao, J., X. Wu, X. Yuan, X. Yang, H. Guo, W. Yao, D. Ji, X. Li, L. Zhang. *Nanocellulose and cellulose making with bio-enzymes from different particle sizes of neosinocalamus affinis*. *Coatings.* **2022**, 12, 1734.
39. Himmel, M.E., J.O. Baker, W.S. Adney, S.R. Decker. *Cellulases, hemicellulases, and pectinases*. *MOJ food process. technol.* **2007**, 596-610.
40. Fenila, F.,Y. Shastri. *Optimal control of enzymatic hydrolysis of lignocellulosic biomass*. *Resour.-Effic. Technol.* **2016**, 2, S96-S104.
41. Jiang, H., J. Nie, L. Zeng, F. Zhu, Z. Gao, A. Zhang, J. Xie, Y. Chen. *Selective Removal of Hemicellulose by Diluted Sulfuric Acid Assisted by Aluminum Sulfate*. *MOL.* **2024**, 29, 2027.
42. Yuan, X., J. Zhao, X. Wu, W. Yao, H. Guo, D. Ji, Q. Yu, L. Luo, X. Li, L. Zhang. *Extraction of corn bract cellulose by the ammonia-coordinated bio-enzymatic method*. *Polymers.* **2022**, 15, 206.
43. Ren, Q., C. Zhao, X. Chen, L. Duan, Y. Li, C. Ma. *NOx and N2O precursors (NH3 and HCN) from biomass pyrolysis: Co-pyrolysis of amino acids and cellulose, hemicellulose and lignin*. *Proc. Combust. Inst.* **2011**, 33, 1715-1722.
44. Mahasweta, L., *Thermochemical Conversion of Biomass to Energy: The Pyrolysis Pathway*, in *The Principles of Green Energy and Technology, Volume 2*. 2025, CRC Press. p. 89-106.
45. Pusceddu, E., A. Montanaro, G. Fioravanti, S. Santilli, P. Foscolo, I. Criscuoli, A. Raschi, F. Miglietta. *Comparison between ancient and fresh biochar samples, a study on the recalcitrance of carbonaceous structures during soil incubation*. *Int. J. New Technol. Res* **2017**, 3, 39-46.
46. Moradi-Choghamarani, F., A.A. Moosavi, M. Baghernejad. *Determining organo-chemical composition of sugarcane bagasse-derived biochar as a function of pyrolysis temperature using proximate and Fourier transform infrared analyses*. *J. Therm. Anal. Calorim.* **2019**, 138, 331-342.
47. Aboelela, D., H. Saleh, A.M. Attia, Y. Elhenawy, T. Majozi, M. Bassyouni. *Recent advances in biomass pyrolysis processes for bioenergy production: optimization of operating conditions*. *Sustainability.* **2023**, 15, 1-30.
48. Duman, G.,J. Yanik. *Two-step steam pyrolysis of biomass for hydrogen production*. *Int. J. Hydrog. Energy.* **2017**, 42, 17000-17008.
49. Pütün, A., N. Özbay, E. Pütün. *Effect of steam on the pyrolysis of biomass*. *Energ. Sources Part A.* **2006**, 28, 253-262.
50. Aro-Modiu, O., M. Osobamiro, A. Osundeko. *Synthesis of graphene oxide from agricultural waste*. *Sci. Afr.* **2019**, 18, 143-151.
51. Sukoyo, A., G. Djoyowasito, Y. Wibisono. *Unravelling the potency of activated carbon powder derived from cultivated marine microalgae as a promising filler in mixed matrix membranes*. *J. Agric. Eng.* **2019**, 1, 188-204.
52. Anthonysamy, S., P. Lahijani, M. Mohammadi, A. Mohamed. *Alkali-modified biochar as a sustainable adsorbent for the low-temperature uptake of nitric oxide*. *Int. J. Environ. Sci. Technol.* **2022**, 19, 7127-7140.
53. Baral, K.R., J. McIlroy, G. Lyons, C. Johnston. *The effect of biochar and acid activated biochar on ammonia emissions during manure storage*. *Environ. Pollut.* **2023**, 317, 120815.
54. Iriarte-Velasco, U., I. Sierra, L. Zudaire, J.L. Ayastuy. *Preparation of a porous biochar from the acid activation of pork bones*. *Food Bioprod. Process.* **2016**, 98, 341-353.
55. Kreuder, A.D., T. House-Knight, J. Whitford, E. Ponnusamy, P. Miller, N. Jesse, R. Rodenborn, S. Sayag, M. Gebel, I. Aped. *A method for assessing greener alternatives between chemical products following the 12 principles of green chemistry*. *ACS Sustain. Chem. Eng.* **2017**, 5, 2927-2935.
56. Lonappan, L., Y. Liu, T. Rouissi, S.K. Brar, R.Y. Surampalli. *Development of biochar-based green functional materials using organic acids for environmental applications*. *J. Clean. Prod.* **2020**, 244, 118841.
57. Eslami, E., S. Carpentieri, G. Pataro, G. Ferrari. *A comprehensive overview of tomato processing by-product valorization by conventional methods versus emerging technologies*. *Foods.* **2022**, 12, 166.
58. Moskovskikh, D. *Overview of Planetary Ball Milling Strategies for Tailoring Composite Powder Morphology and Reactivity*. *Int. J. Self-Propagating High-Temperature Synth.* **2025**, 34, 330-341.

 doi:10.20944/preprints202602.0729.v1

59. Naghdi, M., M. Taheran, S.K. Brar, T. Rouissi, M. Verma, R.Y. Surampalli, J.R. Valero. *A green method for production of nanobiochar by ball milling-optimization and characterization*. *J. Clean. Prod.* **2017**, 164, 1394-1405.
60. Wang, Y., Y. Yu, S. Hu, J. Yu, Y. Huang, H. Dai. *Preparation of Agrowaste-Based Nanocellulose by NaOH-Assisted Ball Milling Technique: Influence of Component Intervention*. *Gels.* **2025**, 11, 631.
61. Phanthong, P., G. Guan, Y. Ma, X. Hao, A. Abudula. *Effect of ball milling on the production of nanocellulose using mild acid hydrolysis method*. *J. Taiwan Inst. Chem. Eng.* **2016**, 60, 617-622.
62. dos Santos, D.F., R.R. Ferreira, A.G. Souza, G.C. Lenhani, V.G. Deon, D.S. Rosa, V.Z. Pinto. *UPCYCLING CORN CROPPING WASTE BY NANOCELLULOSE PRODUCTION*. *Biocatal Agric Biotechnol.* **2025**, 103624.
63. Júnior, J.A.A.,J.B. Baldo. *The behavior of zeta potential of silica suspensions*. *New J. Glass Ceram.* **2014**, 4, 29.
64. Asha, A.B.,R. Narain, *Nanomaterials properties*, in *Polymer science and nanotechnology*. 2020, Elsevier. p. 343-359.
65. Ferreira, R.R., A.G. Souza, L.L. Nunes, N. Shahi, V.K. Rangari, D. dos Santos Rosa. *Use of ball mill to prepare nanocellulose from eucalyptus biomass: challenges and process optimization by combined method*. *Mater. Today Commun.* **2020**, 22, 100755.
66. Hoseinpour, Z., R. Niazmand, M. Heydari-Majd. *Extraction and characterization of nanocellulose from Cuminum cyminum L. husk by ball-milling-assisted ultrasound*. *Carbohydr. Polym. Technol. Appl.* **2025**, 100934.
67. Nakatuka, Y., H. Yoshida, K. Fukui, M. Matuzawa. *The effect of particle size distribution on effective zeta-potential by use of the sedimentation method*. *Adv. Powder Technol.* **2015**, 26, 650-656.
68. Saleh, T.A. *Nanomaterials: Classification, properties, and environmental toxicities*. *Environ. Technol. Innov.* **2020**, 20, 101067.
69. Serrano-Lotina, A., R. Portela, P. Baeza, V. Alcolea-Rodríguez, M. Villarroel, P. Ávila. *Zeta potential as a tool for functional materials development*. *Catal. Today.* **2023**, 423, 113862.
70. Ali, W.A., S.E. Richards, R.H. Alzard. *Unlocking the potential of ball milling for nanomaterial Synthesis: An overview*. *J. Ind. Eng. Chem.* **2025**,
71. Yadav, T.P., R.M. Yadav, D.P. Singh. *Mechanical milling: a top down approach for the synthesis of nanomaterials and nanocomposites*. *J. Nanosci. Nanotechnol.* **2012**, 2, 22-48.
72. Du Plessis, M. *Relationship between specific surface area and pore dimension of high porosity nanoporous silicon–model and experiment*. *Phys. Status Solidi A.* **2007**, 204, 2319-2328.
73. Tessema, B., G. Gonfa, S. Mekuria Hailegiorgis, S. Venkatesa Prabhu. *An overview of current and prognostic trends on synthesis, characterization, and applications of biobased silica*. *Adv. mater. sci. eng.* **2023**, 2023, 4865273.
74. Liu, Z., J. Li, Q. Wang, X. Lu, Y. Zhang, M. Zhu, Z. Zhang, D. Zhang. *An experimental investigation into mineral transformation, particle agglomeration and ash deposition during combustion of Zhundong lignite in a laboratory-scale circulating fluidized bed*. *Fuel.* **2019**, 243, 458-468.
75. Antony Jose, S., N. Cowan, M. Davidson, G. Godina, I. Smith, J. Xin, P.L. Menezes. *A comprehensive review on cellulose Nanofibers, nanomaterials, and composites: Manufacturing, properties, and applications*. *Nanomaterials.* **2025**, 15, 356.
76. Kondor, A., A. Santmarti, A. Mautner, D. Williams, A. Bismarck, K.-Y. Lee. *On the BET surface area of nanocellulose determined using volumetric, gravimetric and chromatographic adsorption methods*. *Front. Chem. Eng.* **2021**, 3, 738995.
77. Osorio, M., P. Fernández-Morales, P. Gañán, R. Zuluaga, H. Kerguelen, I. Ortiz, C. Castro. *Development of novel three-dimensional scaffolds based on bacterial nanocellulose for tissue engineering and regenerative medicine: Effect of processing methods, pore size, and surface area*. *J. Biomed. Mater. Res. A.* **2019**, 107, 348-359.
78. Krishnaiah, P., C.T. Ratnam, S. Manickam. *Enhancements in crystallinity, thermal stability, tensile modulus and strength of sisal fibres and their PP composites induced by the synergistic effects of alkali and high intensity ultrasound (HIU) treatments*. *Ultrason. Sonochem.* **2017**, 34, 729-742.
79. Rana, M.S., M.A. Rahim, M.P. Mosharraf, M.F.K. Tipu, J.A. Chowdhury, M.R. Haque, S. Kabir, M.S. Amran, A.A. Chowdhury. *Morphological, spectroscopic and thermal analysis of cellulose nanocrystals extracted from waste jute fiber by acid hydrolysis*. *Polymers.* **2023**, 15, 1530.
80. Moon, R., L. Johnston, C. Land-Hensdal, W. Batchelor. *Perspectives on cellulose nanofibril size measurement using scanning electron microscopy*. *Cellul.* **2025**, 1-18.

 doi:10.20944/preprints202602.0729.v1

81. Mehanny, S., E.E. Abu-El Magd, M. Ibrahim, M. Farag, R. Gil-San-Millan, J. Navarro, A.E.H. El Habbak, E. El-Kashif. *Extraction and characterization of nanocellulose from three types of palm residues*. *J. Mater. Res. Technol.* **2021**, 10, 526-537.
82. Schroeder, A.B., E.T. Dobson, C.T. Rueden, P. Tomancak, F. Jug, K.W. Eliceiri. *The ImageJ ecosystem: Open-source software for image visualization, processing, and analysis*. *Protein Sci.* **2021**, 30, 234-249.
83. Hotaling, N.A., K. Bharti, H. Kriel, C.G. Simon Jr. *DiameterJ: A validated open source nanofiber diameter measurement tool*. *Biomaterials.* **2015**, 61, 327-338.
84. Ho, H.V., P. Makkar, A.R. Padalhin, T.T.T. Le, S.Y. Lee, G. Jaegyoung, B.-T. Lee. *Preliminary studies on the in vivo performance of various kinds of nanocellulose for biomedical applications*. *J. Biomater. Appl.* **2020**, 34, 942-951.
85. Tarrés, Q., R. Aguado, J.O. Zoppe, P. Mutjé, N. Fiol, M. Delgado-Aguilar. *Dynamic light scattering plus scanning electron microscopy: usefulness and limitations of a simplified estimation of nanocellulose dimensions*. *Nanomaterials.* **2022**, 12, 4288.
86. Wang, L., B. Liu, H. Li, W. Yang, Y. Ding, S.V. Sinogeikin, Y. Meng, Z. Liu, X.C. Zeng, W.L. Mao. *Long-range ordered carbon clusters: a crystalline material with amorphous building blocks*. *J. Sci.* **2012**, 337, 825-828.
87. Du, H., K. Liu, T. Xu, C. Xu, M. Lin, Z. Fang, S.-W. Kim, J.-Y. Seo, J. Chen, H. Ma. *Lignocellulosic Films: Preparation, Properties, and Applications*. *Chem. Rev.* **2025**,
88. Santmartí, A.,K.-Y. Lee, *Crystallinity and thermal stability of nanocellulose*, in *Nanocellulose and sustainability*. 2018, CRC Press. p. 67-86.
89. Nam, S., Y. Liu, Z. He, D.J. Hinchliffe, D. Fang. *Assessment of Segal method for identifying crystallinity evolution in developing cotton fibers*. *Agric. environ. lett.* **2024**, 9, e20138.
90. Rashid, S.,H. Dutta. *Characterization of nanocellulose extracted from short, medium and long grain rice husks*. *Ind. Crop. Prod.* **2020**, 154, 112627.
91. Raza, M., B. Abu-Jdayil, F. Banat, A.H. Al-Marzouqi. *Isolation and characterization of cellulose nanocrystals from date palm waste*. *ACS Omega.* **2022**, 7, 25366-25379.
92. Seifert, E., *OriginPro 9.1: Scientific data analysis and graphing software–software review*. 2014, ACS Publications.
93. Verma, Y.K., A.K. Singh, M. Paswan, P.K. Gurmaita. *Preparation and characterization of bamboo based nanocellulose by ball milling and used as a filler for preparation of nanocomposite*. *Polymer.* **2024**, 308, 127396.
94. Phanthong, P., S. Karnjanakom, P. Reubroycharoen, X. Hao, A. Abudula, G. Guan. *A facile one-step way for extraction of nanocellulose with high yield by ball milling with ionic liquid*. *Cellul.* **2017**, 24, 2083-2093.
95. Lichtenstein, K.,N. Lavoine. *Toward a deeper understanding of the thermal degradation mechanism of nanocellulose*. *Polym. Degrad. Stabil.* **2017**, 146, 53-60.
96. Ballesteros-Mártinez, L., C. Pérez-Cervera, R. Andrade-Pizarro. *Effect of glycerol and sorbitol concentrations on mechanical, optical, and barrier properties of sweet potato starch film*. *NFS J.* **2020**, 20, 1-9.
97. Bonifacio, A., L. Bonetti, E. Piantanida, L. De Nardo. *Plasticizer design strategies enabling advanced applications of cellulose acetate*. *Eur. Polym. J.* **2023**, 197, 112360.
98. Sanyang, M.L., S.M. Sapuan, M. Jawaid, M.R. Ishak, J. Sahari. *Effect of plasticizer type and concentration on tensile, thermal and barrier properties of biodegradable films based on sugar palm (Arenga pinnata) starch*. *Polymers.* **2015**, 7, 1106-1124.
99. Shin, S. *Rheological Design and Applications of Cellulose Nanofiber in Additive Manufacturing*. *J. of Korea TAPPI.* **2025**, 57, 19-31.
100. Ospennikov, A.S., A.L. Kwiatkowski, O.E. Philippova. *Cellulose nanofibrils vs nanocrystals: Rheology of suspensions and hydrogels*. *Gels.* **2025**, 11, 926.
101. Ait Balla, M., A. Maazouz, K. Lamnawar, F.E. Arrakhiz. *Biowastes as Reinforcements for Sustainable PLA-Biobased Composites Designed for 3D Printing Applications: Structure–Rheology–Process–Properties Relationships*. *Polymers.* **2025**, 18, 128.
102. Aigaje, E., A. Riofrio, H. Baykara. *Processing, properties, modifications, and environmental impact of nanocellulose/biopolymer composites: a review*. *Polymers.* **2023**, 15, 1-19.
103. Shojaeiarani, J., D.S. Bajwa, N.M. Stark, S.G. Bajwa. *Rheological properties of cellulose nanocrystals engineered polylactic acid nanocomposites*. *Compos. B Eng.* **2019**, 161, 483-489.

 doi:10.20944/preprints202602.0729.v1

104. Meng, W., X. Zhang, X. Hu, Y. Liu, J. Zhang, X. Qu, B. Abdel-Magid. *Mechanical Properties and Non-Isothermal Crystallization Kinetics of Polylactic Acid Modified by Polyacrylic Elastomers and Cellulose Nanocrystals*. *Polymers.* **2023**, 15, 3767.
105. Tang, K., S. Wang, H. Liu, C. Zhang, Y. Yao, S. Lu, X. Liao. *Manipulation of crystallization nucleation and mechanical properties of PBAT films by octadecylamine-cellulose*. *ACS Sustain. Chem. Eng.* **2024**, 12, 4276-4285.
106. Alonso-Cañon, S., A. Alonso-Estébanez, A.I. Yoris-Nobile, A. Brunčič, E. Blanco-Fernandez, L. Castanon-Jano. *Rheological parameter ranges for 3D printing sustainable mortars using a new low-cost rotational rheometer*. *Int. J. Adv. Manuf. Tech.* **2025**, 140, 1945-1961.
107. Lasseuguette, E., D. Roux, Y. Nishiyama. *Rheological properties of microfibrillar suspension of TEMPO-oxidized pulp*. *Cellul.* **2008**, 15, 425-433.
108. Gharib, N., B. Bharathan, L. Amiri, M. McGuinness, F.P. Hassani, A.P. Sasmito. *Flow characteristics and wear prediction of Herschel-Bulkley non-Newtonian paste backfill in pipe elbows*. *Can. J. Chem. Eng.* **2017**, 95, 1181-1191.
109. Zou, L., M. Tang, B. Li. *Bingham and herschel-bulkley fluids flow regimes in rough-walled rock fractures*. *Int. J. Rock Mech. Min. Sci.* **2024**, 180, 105832.
110. Mahmood, F.T., T.S. Chowdhury, M.N. Hasan. *Fluid-structure interaction induced mixed convection characteristics in a lid-driven square cavity with non-Newtonian power law fluids*. *Int. J. Thermofluids.* **2024**, 22, 100687.
111. Nabels-Sneiders, M., A. Barkane, O. Platnieks, L. Orlova, S. Gaidukovs. *Biodegradable poly (butylene succinate) laminate with nanocellulose interphase layer for high-barrier packaging film application*. *Foods.* **2023**, 12, 4136.
112. Ren, Y., X. Fan, L. Cao, Y. Chen. *Water-resistant and barrier properties of poly (vinyl alcohol)/nanocellulose films enhanced by metal ion crosslinking*. *Int. J. Biol. Macromol.* **2024**, 277, 134245.
113. Riaz, T., X. Zeng, X. Ye, T. Yu, Z. Xia, M.M. Khan, T. Ahmad, A. Kalsoom, M.A. Rauf, M.A. Ashraf. *The Biophysics of Nanocellulose Packaging: Linking Nanoscale Structure to Food Preservation and Safety*. *Food Biophys.* **2025**, 20, 196.
114. Yu, K., L. Yang, S. Zhang, N. Zhang, D. Zhu, Y. He, X. Cao, H. Liu. *Tough, antibacterial, antioxidant, antifogging and washable chitosan/nanocellulose-based edible coatings for grape preservation*. *Food Chem.* **2025**, 468, 142513.
115. Zhang, L., M. Cui, H. Tong, J. Zhang, Q. Li, X. Gao, W. Qi, H.L. Lam, R. Huang, R. Su. *Multi-functional edible coatings tailored with nanocellulose for perishable fruits*. *Carbohydr. Polym.* **2025**, 358, 123520.
116. Zhao, J., J. Cai, Y. Huang, J. Luo. *Nanocellulose-based carbon sphere immobilized AgNPs for antibacterial cellulosic paper*. *Ind. Crop. Prod.* **2025**, 230, 121120.
117. Zhang, K., C. Li, L. Liu, X. Wang, N. Li, C. Yang, Y. Huang, H. Lu, H. Liu, J. Li. *Developing lightweight silanized cellulose ultramaterials as the strongest engineered aerogel*. *Adv. Funct. Mater.* **2025**, 35, 2415963.
118. Alves, Z., P. Brites, N.M. Ferreira, G. Figueiredo, G. Otero-Irurueta, I. Gonçalves, S. Mendo, P. Ferreira, C. Nunes. *Thermoplastic starch-based films loaded with biochar-ZnO particles for active food packaging*. *J. Food Eng.* **2024**, 361, 111741.
119. Feng, Q., B. Fan, Y.-C. He, C. Ma. *Antibacterial, antioxidant and fruit packaging ability of biochar-based silver nanoparticles-polyvinyl alcohol-chitosan composite film*. *Int. J. Biol. Macromol.* **2024**, 256, 128297.
120. Hubbe, M.A., P. Tayeb, M. Joyce, P. Tyagi, M. Kehoe, K. Dimic-Misic, L. Pal. *Rheology of nanocellulose-rich aqueous suspensions: a review*. *BioResources.* **2017**, 12, 9556-9661.
121. Wu, J., Y. Gao, H. Shen, S. Yan, R. Zhao, F. Wang, X. Shen, Z. Li, X. Yao, Y. Wang. *Application potential of wheat bran cellulose nanofibers as Pickering emulsion stabilizers and stabilization mechanisms*. *Food Chem. X.* **2024**, 24, 101922.
122. Wu, J., X. Tang, W. Gao, J. Li, J. Li, D. Cao, J. Zeng, B. Wang, J. Xu, K. Chen. *Excellently stable Camellia oleifera oil Pickering emulsion fabricated based on high carboxyl content cellulose nanofibrils*. *Carbohydr. Polym.* **2025**, 123694.
123. Zhang, Z., X. Lin, J. Lin, N. Liu, B. Wan, X. Fang, L. Shui, Y. Li, K.C. Tam, J. Huang. *Cellulose supported and strengthened shear stiffening gel with enhanced impact-resistant performance*. *Chem. Eng. J.* **2023**, 473, 145435.

 doi:10.20944/preprints202602.0729.v1

124. Hamouda, R.A., F.A. Qarabai, F.S. Shahabuddin, T.M. Al-Shaikh, R.R. Makharita. *Antibacterial activity of ulva/nanocellulose and ulva/Ag/cellulose nanocomposites and both blended with fluoride against bacteria causing dental decay*. *Polymers.* **2023**, 15, 1047.
125. Hafid, H.S., F.N. Omar, J. Zhu, M. Wakisaka. *Enhanced crystallinity and thermal properties of cellulose from rice husk using acid hydrolysis treatment*. *Carbohydr. Polym.* **2021**, 260, 117789.
126. Ponce, J., J.G. da Silva Andrade, L.N. dos Santos, M.K. Bulla, B.C.B. Barros, S.L. Favaro, N. Hioka, W. Caetano, V.R. Batistela. *Alkali pretreated sugarcane bagasse, rice husk and corn husk wastes as lignocellulosic biosorbents for dyes*. *Carbohydr. Polym. Technol. Appl.* **2021**, 2, 100061.
127. Vu, A.N., L.H. Nguyen, H.-C.V. Tran, K. Yoshimura, T.D. Tran, H. Van Le, N.-U.T. Nguyen. *Cellulose nanocrystals extracted from rice husk using the formic/peroxyformic acid process: isolation and structural characterization*. *RSC Adv.* **2024**, 14, 2048-2060.
128. Lin, L., Y. E, Q. Sun, Y. Chen, W. Dai, Z. Bao, W. Niu, J. Meng. *Analysis of the pyrolysis kinetics, reaction mechanisms, and by-products of Rice husk and rice straw via TG-FTIR and Py-GC/MS*. *MOL.* **2024**, 30, 10.
129. Rodríguez-Chong, A., J.A. Ramírez, G. Garrote, M. Vázquez. *Hydrolysis of sugar cane bagasse using nitric acid: a kinetic assessment*. *J. Food Eng.* **2004**, 61, 143-152.
130. Mahmud, M.A.,F.R. Anannya. *Sugarcane bagasse-A source of cellulosic fiber for diverse applications*. *Heliyon.* **2021**, 7,
131. Song, G., M. Madadi, X. Meng, C. Sun, M. Aghbashlo, F. Sun, A.J. Ragauskas, M. Tabatabaei, A. Ashori. *Double in-situ lignin modification in surfactant-assisted glycerol organosolv pretreatment of sugarcane bagasse towards efficient enzymatic hydrolysis*. *Chem. Eng. J.* **2024**, 481, 148713.
132. Husna, M.,S. Vasantharuba. *Analysis and comparison of peanut shell's cellulose content*. **2022**,
133. Anike, F., M. Yusuf, O. Isikhuemhen. *Co-substrating of peanut shells with cornstalks enhances biodegradation by Pleurotus ostreatus*. *J Bioremed Biodeg.* **2016**, 7, 1-7.
134. Pączkowski, P., A. Puszka, B. Gawdzik. *Effect of eco-friendly peanut shell powder on the chemical resistance, physical, thermal, and thermomechanical properties of unsaturated polyester resin composites*. *Polymers.* **2021**, 13, 3690.
135. Garcia-Maraver, A., D. Salvachúa, M. Martínez, L. Diaz, M. Zamorano. *Analysis of the relation between the cellulose, hemicellulose and lignin content and the thermal behavior of residual biomass from olive trees*. *Waste Manag.* **2013**, 33, 2245-2249.
136. Mansora, A.M., J.S. Lima, F.N. Anib, H. Hashima, W.S. Hoa. *Characteristics of cellulose, hemicellulose and lignin of MD2 pineapple biomass*. *Chem. Eng.* **2019**, 72, 79-84.
137. Daud, Z., H. Awang, A.S.M. Kassim, M.Z.M. Hatta, A.M. Aripin. *Comparison of pineapple leaf and cassava peel by chemical properties and morphology characterization*. *Adv. Mater. Res.* **2014**, 974, 384-388.
138. Aripin, A.M., A.S.M. Kassim, Z. Daud, M.Z.M. Hatta. *Cassava peels for alternative fibre in pulp and paper industry: chemical properties and morphology characterization*. *Int. J. Integr. Eng.* **2013**, 5,
139. Mubarik, S., N. Qureshi, Z. Sattar, A. Shaheen, A. Kalsoom, M. Imran, F. Hanif. *Synthetic approach to rice waste-derived carbon-based nanomaterials and their applications*. *J. Nanomanuf.* **2021**, 1, 109-159.
140. Liu, J., Y. Xue, M. Zhang, L. Dai. *Graphene-based materials for energy applications*. *MRS Bull.* **2012**, 37, 1265-1272.
141. Terea, H., D. Selloum, A. Rebiai, A. Bouafia, O. Ben Mya. *Preparation and characterization of cellulose/ZnO nanoparticles extracted from peanut shells: effects on antibacterial and antifungal activities*. *Biomass Convers. Biorefin.* **2024**, 14, 19489-19500.
142. Abdul Rahman, N.H., B.W. Chieng, N.A. Ibrahim, N. Abdul Rahman. *Extraction and characterization of cellulose nanocrystals from tea leaf waste fibers*. *Polymers* **2017**, 9, 588.
143. Guo, Y., Y. Zhang, D. Zheng, M. Li, J. Yue. *Isolation and characterization of nanocellulose crystals via acid hydrolysis from agricultural waste-tea stalk*. *Int. J. Biol. Macromol.* **2020**, 163, 927-933.
144. Abdul Rahman, N.H., B.W. Chieng, N.A. Ibrahim, N. Abdul Rahman. *Extraction and characterization of cellulose nanocrystals from tea leaf waste fibers*. *Polymers.* **2017**, 9, 1-11.
145. Mohd, N.K., N.N.A.N. Wee, A.A. Azmi. *Green synthesis of silica nanoparticles using sugarcane bagasse*. in *AIP conference proceedings*. 2017. AIP Publishing LLC.

 doi:10.20944/preprints202602.0729.v1

146. Pelissari, F.M., M.M. Andrade-Mahecha, P.J. do Amaral Sobral, F.C. Menegalli. *Nanocomposites based on banana starch reinforced with cellulose nanofibers isolated from banana peels*. *J. Colloid Interface Sci.* **2017**, 505, 154-167.
147. Paras, K. Yadav, P. Kumar, D.R. Teja, S. Chakraborty, M. Chakraborty, S.S. Mohapatra, A. Sahoo, M.M. Chou, C.-T.J.N. Liang. *A review on low-dimensional nanomaterials: nanofabrication, characterization and applications*. **2022**, 13, 160.
148. Su, B., Y. Wu, L. Jiang. *The art of aligning one-dimensional (1D) nanostructures*. *Chem. Soc. Rev.* **2012**, 41, 7832-7856.
149. Li, X.,J. Wang. *One-dimensional and two-dimensional synergized nanostructures for high-performing energy storage and conversion*. *InfoMat.* **2020**, 2, 3-32.
150. Dutta, S., J. Kim, Y. Ide, J.H. Kim, M.S.A. Hossain, Y. Bando, Y. Yamauchi, K.C.-W. Wu. *3D network of cellulose-based energy storage devices and related emerging applications*. *Mater. Horiz.* **2017**, 4, 522-545.
151. Sumarago, E.C., M.F.M. dela Cerna, A.K.B. Leyson, N.P.B. Tan, K.F. Magsico. *Production and characterization of nanocellulose from maguey (Agave cantala) fiber*. *Polymers.* **2024**, 16, 1312.
152. Hossain, M.I., M.M. Rahman, B.C. Ghos, M.A. Gafur, M.A. Alam, M.A. Rabbi. *Preparation and characterization of crystalline nanocellulose from keya (Pandanus tectorius) L. fiber as potential reinforcement in sustainable bionanocomposite: A waste to wealth scheme*. *Carbohydr. Polym. Technol. Appl.* **2024**, 8, 100600.
153. Punnadiyil, R.K., M. Sreejith, E. Purushothaman. *Isolation of microcrystalline and nano cellulose from peanut shells*. *J. Chem. Pharm. Sci.* **2016**, 974, 2115.
154. Mishra, S., B. Prabhakar, P.S. Kharkar, A.M. Pethe. *Banana peel waste: An emerging cellulosic material to extract nanocrystalline cellulose*. *ACS Omega.* **2022**, 8, 1140-1145.